Rac1 and Aurora A regulate MCAK to polarize microtubule growth in migrating endothelial cells

Alexander Braun,[1] Kyvan Dang,[1] Felinah Buslig,[1] Michelle A. Baird,[3,4] Michael W. Davidson,[3,4] Clare M. Waterman,[2] and Kenneth A. Myers[1,2]

[1]Department of Biological Sciences, University of the Sciences, Philadelphia, PA 19104
[2]Cell Biology and Physiology Center, National Heart, Lung and Blood Institute, National Institutes of Health, Bethesda, MD 20892
[3]National High Magnetic Field Laboratory and [4]Department of Biological Science, The Florida State University, Tallahassee, FL 32310

Endothelial cells (ECs) migrate directionally during angiogenesis and wound healing by polarizing to extracellular cues to guide directional movement. EC polarization is controlled by microtubule (MT) growth dynamics, which are regulated by MT-associated proteins (MAPs) that alter MT stability. Mitotic centromere-associated kinesin (MCAK) is a MAP that promotes MT disassembly within the mitotic spindle, yet its function in regulating MT dynamics to promote EC polarity and migration has not been investigated. We used high-resolution fluorescence microscopy coupled with computational image analysis to elucidate the role of MCAK in regulating MT growth dynamics, morphology, and directional migration of ECs. Our results show that MCAK-mediated depolymerization of MTs is specifically targeted to the trailing edge of polarized wound-edge ECs. Regulation of MCAK function is dependent on Aurora A kinase, which is regionally enhanced by signaling from the small guanosine triphosphatase, Rac1. Thus, a Rac1–Aurora A–MCAK signaling pathway mediates EC polarization and directional migration by promoting regional differences in MT dynamics in the leading and trailing cell edges.

Introduction

Angiogenesis is triggered by extracellular cues that promote endothelial cell (EC) invasion and migration into tissues that require blood supply. These signals induce ECs to polarize and undergo morphogenesis in which they extend new cell branches with directional specificity to guide directional movement in formation of the vascular network (Gerhardt et al., 2003, 2004; Gerhardt and Betsholtz, 2005). EC branching morphogenesis is critically dependent on the dynamic and coordinated regulation of the actomyosin and microtubule (MT) cytoskeletons (Bayless and Johnson, 2011). Myosin II contractility negatively regulates EC branch formation (Fischer et al., 2009), whereas MT growth dynamics are required for EC branching, and MTs grow slowly and persistently to support existing branches (Myers et al., 2011). In this way, ECs modify their cytoskeleton to polarize their morphology to facilitate directional migration.

Polarization of MT assembly dynamics within the cell is critical to achieving a polarized cell morphology (Rodriguez et al., 2003). For example, in migrating epithelial cells, cell polarization is mediated by the promotion of "pioneer" MTs that grow slowly and persistently specifically at the leading edge of the cell (Waterman-Storer et al., 1999; Wittmann et al., 2003). In neurons, polarized MT growth dynamics are required for the elongation of branch-like neurites, which later become defined as axons or dendrites (Ahmad et al., 1993, Dent et al., 1999; Dent and Kalil, 2001). Inhibition of MT growth dynamics is sufficient to eliminate axon elongation and contributes to the retraction of existing neuronal arbors (Van Veen and Van Pelt, 1994; Dehmelt and Halpain, 2004; Dehmelt et al., 2006; Myers et al., 2006). Thus, regional control of MT growth dynamics is used to modulate shape and drive polarization across many cell types.

A key mechanism used by cells to control MT growth dynamics is the regulation of MT-associated proteins (MAPs). MAPs include molecular motor and nonmotor proteins that

Correspondence to Kenneth Myers: k.myers@usciences.edu; or Clare M. Waterman: watermancm@nhlbi.nih.gov

Abbreviations used in this paper: CA, constitutively active; DN, dominant negative; EB3, end-binding protein 3; EC, endothelial cell; Em, mEmerald; HUVEC, human umbilical vein EC; MAP, MT-associated protein; MCAK, mitotic centromere-associated kinesin; MT, microtubule; ROI, region of interest.

The Rockefeller University Press $30.00
J. Cell Biol. Vol. 206 No. 1 97–112
www.jcb.org/cgi/doi/10.1083/jcb.201401063

function to directly regulate the stability of the MT array by changing the dynamics of MT growth and disassembly. The functions of MAPs in regulating MT dynamics are controlled through spatiotemporal inhibition or activation, which provides the cell a mechanism to locally regulate MT dynamics and thereby promote cell polarization (Wittmann and Waterman-Storer, 2005; Kumar et al., 2009; Al-Bassam and Chang, 2011). Key signaling cascades mediated by the Rho family of small GTPases are critical to regulating MT dynamics through the regulation of MAPs. For example, the Rac1 GTPase has been shown to promote pioneer MT growth via downstream targets such as Op18/stathmin and CLASPs that directly bind tubulin or MTs to regulate MT assembly dynamics (Wittmann et al., 2003, 2004; Wittmann and Waterman-Storer, 2005). However, additional Rac1 targets that regulate MT polarization in cells remain to be identified.

Mitotic centromere-associated kinesin (MCAK) is a Kinesin-13 family MAP that binds to MT ends and couples ATP hydrolysis to MT disassembly (Desai et al., 1999; Hunter et al., 2003, Lee et al., 2008). In mitosis, MCAK localizes to spindle poles and kinetochores, where it promotes proper spindle assembly and separation of sister chromatids during anaphase (Walczak et al., 1996; Maney et al., 1998; Lan et al., 2004; Ganem et al., 2005; Wordeman et al., 2007). In interphase, MCAK localizes to and tracks with growing MT plus ends and enhances MT disassembly (Kline-Smith and Walczak, 2002; Moore et al., 2005). Localization and activity of MCAK are controlled by phosphorylation at multiple sites by Aurora family kinases. Phosphorylation by either Aurora A or B on serine 196 promotes MCAK inactivation. In mitosis, this regulation is required for proper spindle formation and chromosome segregation (Ohi et al., 2004, Mennella et al., 2005; Knowlton et al., 2006; Zhang et al., 2007, 2008). In contrast, the regulation of MCAK in interphase cells is less well studied. Although Aurora B is sequestered in the nucleus during interphase, Aurora A is cytoplasmic during interphase (Rannou et al., 2008), and specific inhibition of Aurora A inhibits MT disassembly (Lorenzo et al., 2009). However, it is not known whether Aurora A regulates the MT disassembling activity of MCAK during interphase and whether this mediates polarization of EC morphology and directional cell migration.

Here we used high-resolution fluorescence microscopy coupled with computational image analysis of fluorescently labeled MT plus ends to investigate the role of MCAK in MT growth dynamics and the regulation of EC branching morphology and directional migration. We find that MCAK is required for EC branching and directional migration and that MCAK specifically promotes MT disassembly in the cell trailing edge. Additionally, we find that down-regulation of MCAK function is Aurora A kinase dependent and requires phosphorylation of MCAK specifically at Serine 196. We further show that Aurora A kinase activity is regionally enhanced at the leading edge and regulated by signaling from the small GTPase Rac1. Thus, a Rac1–Aurora A–MCAK signaling pathway mediates EC polarization and directional migration by promoting regional differences in MT dynamics in the leading and trailing cell edges.

Results

MCAK limits MT growth to regulate endothelial cell branching morphogenesis and directional migration

We first set out to confirm that MCAK tracks with growing MT plus ends and promotes MT depolymerization in human umbilical vein ECs (HUVECs), as has been shown in other cell types (Moore et al., 2005). Labeling of tubulin in cells overexpressing GFP-tagged MCAK revealed depolymerization of the cytoplasmic MT array to near completion (Fig. 1 A). Coexpression of GFP-MCAK with mApple fluorescent protein fused to MT end-binding protein 3 (EB3; mApple-EB3) followed by live-cell imaging revealed that in cells expressing low levels, GFP-MCAK tracked with EB3-labeled, growing MT plus ends in HUVECs (Fig. 1, B and C; and Video 1), confirming results observed in other cell types (Moore et al., 2005).

We next sought to determine the effects of MCAK on MT dynamics in HUVECs. We performed live-cell imaging of mApple-EB3 in HUVECs with perturbed MCAK expression levels. HUVECs were transfected with mApple-EB3 together with control shRNA, MCAK shRNA, GFP-MCAK, or MCAK shRNA rescued with GFP-MCAK expression (Rescue). Transfection efficiencies for GFP-MCAK and mApple-EB3 were 44 ± 4%, whereas for MCAK shRNA it was 61 ± 6%. Densitometry quantification of Western blots 6 h posttransfection revealed that shRNA treatment reduced the level of MCAK by 65 ± 4%, and that this could be rescued to 88 ± 3% of endogenous levels by reexpression of GFP-MCAK, whereas overexpression of GFP-MCAK enhanced MCAK levels by 146 ± 2% relative to untransfected controls (Fig. 1 I).

We measured MT growth speed and growth lifetimes in time-lapse images of mApple-EB3 dynamics in cells with altered expression levels using automated image analysis with plusTipTracker software, as described previously (Myers et al., 2011). Because plusTipTracker software is uniquely designed to track MT growth parameters, our analysis throughout this study included only measurements of the speed (micrometers/second) and lifetime of MT growth (seconds from EB3 track origin to EB3 track disappearance). Data output from plusTipTracker includes image overlays of MT plus end motion tracks, with the magnitudes of MT growth speed and growth lifetime color coded to allow qualitative visualization of regional differences in these values throughout the cell (Fig. 1, D–H). In addition, data from individual cells or user-defined subcellular regions of interest can be pooled to allow statistical analysis of changes in MT growth speed and growth lifetime under different experimental conditions or in different subcellular regions.

Image overlays of MT plus end motion tracks showed that depletion of MCAK induced long-lived MT growth throughout the cell (Fig. 1 F, blue and green tracks) with slow long-lived growth concentrated in the cell periphery (green tracks). Expression of GFP-MCAK promoted very short-lived MT growth excursions (Fig. 1 G, yellow and red tracks), whereas rescue of MCAK knockdown (Fig. 1 H) resulted in MT plus end motion tracks that were similar to controls (Fig. 1 E). Quantitation of MT growth tracks showed that MCAK

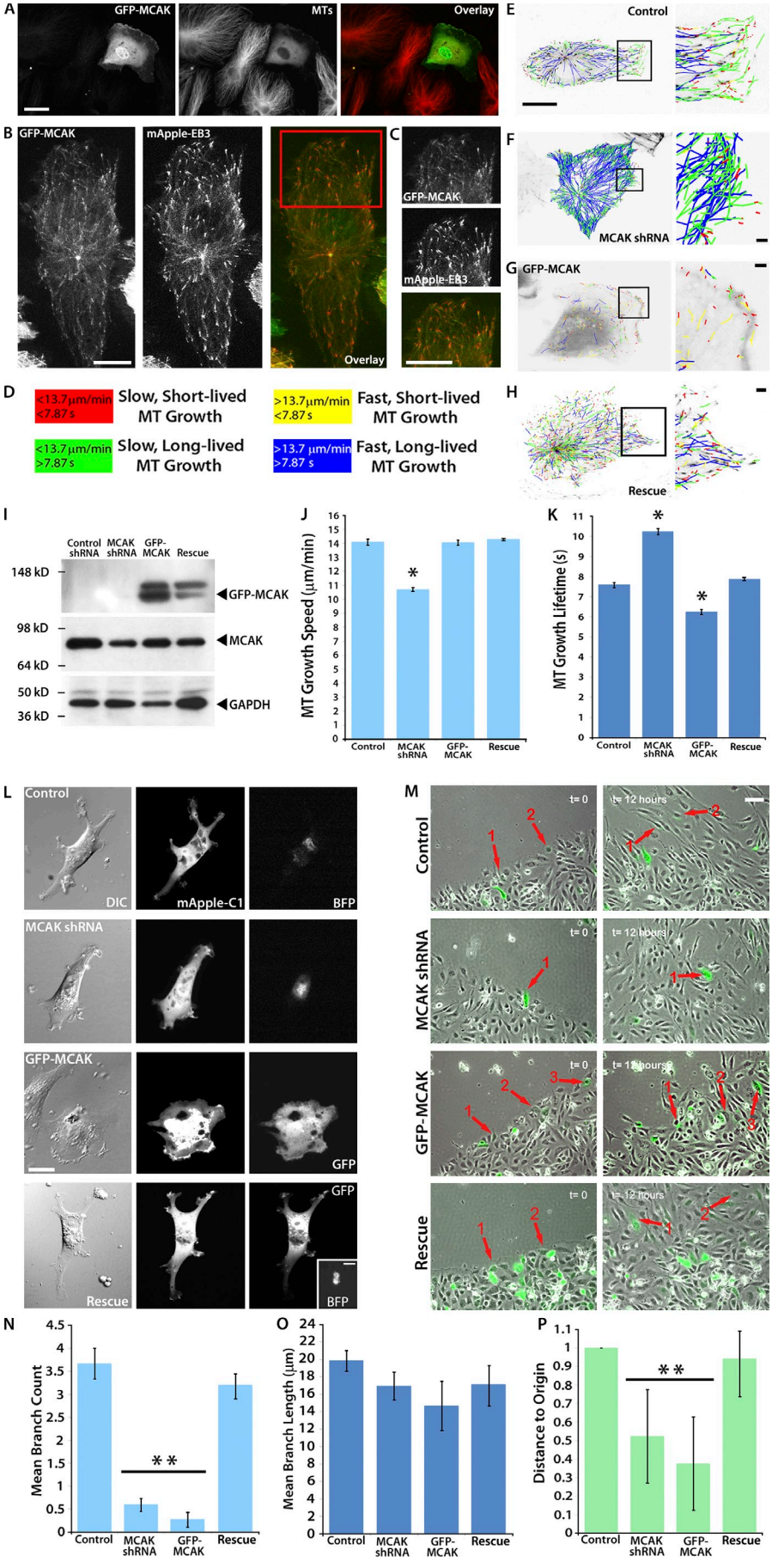

Figure 1. **MCAK limits MT growth to regulate EC branching morphogenesis and directional migration.** (A) A HUVEC at the edge of a monolayer wound overexpressing GFP-MCAK and immunolabeled for α-tubulin displays few MTs compared with untransfected cells. (B and C) A wound-edge HUVEC expressing low levels of GFP-MCAK (green). GFP-MCAK tracks with growing, mApple-EB3–labeled MT plus ends (red) in HUVECs (see also Video 1). (C) Zoom of red-boxed region in B highlights GFP-MCAK and mApple-EB3 colocalization. In A–C, the wound edge faces up. (D) MT tracks shown in E–H are color coded according to their growth speed and lifetime. (E–H), MT growth tracks from 2-min time-lapse videos of mApple-EB3 (2-s intervals) from plusTipTracker software. Whole cells (left) and zoom of boxed regions (right). (E) HUVEC expressing control shRNA. (F) HUVEC expressing shRNA targeting MCAK. (G) HUVEC expressing GFP-MCAK. (H) HUVEC expressing MCAK shRNA and GFP-MCAK (Rescue). (I) Western blot of HUVEC lysates for MCAK in untreated (control) or MCAK shRNA-, GFP-MCAK-, or Rescue-treated HUVECs. (J and K) Comparison of mean MT growth speeds (J) and mean MT growth excursion lifetimes (K) from mApple EB3 tracks for control, MCAK shRNA-, GFP-MCAK–, or Rescue-treated HUVECs. (L) DIC images of HUVECs plated on 0.7 kPa fibronectin-coupled polyacrylamide substrates to induce cell branching. Cells were expressing a fluorescent volume marker (mApple-C1) and either BFP-control shRNA, BFP-MCAK shRNA, GFP-MCAK, or Rescue. (M) Phase-contrast images of BFP-control shRNA, BFP-MCAK shRNA, or GFP-MCAK–expressing HUVECs migrating in an experimentally induced wound. Fluorescence (green) and red arrows point to wound-edge GFP-expressing cells at the start point (left) and end point (right) of the migration assay. (N–P) Quantification of HUVEC branch number per cell (N) and branch length (O). (P) Quantification of directional migration in a wound-edge migration assay. Bars: (A and L) 25 μm; (L, inset) 10 μm; (B–H, main) 10 μm; (B–H, zoomed) 2 μm; (M) 50 μm. *, $P < 0.001$; **, $P < 0.05$. Error bars show ± standard error in J and K and ± standard deviation in N–P.

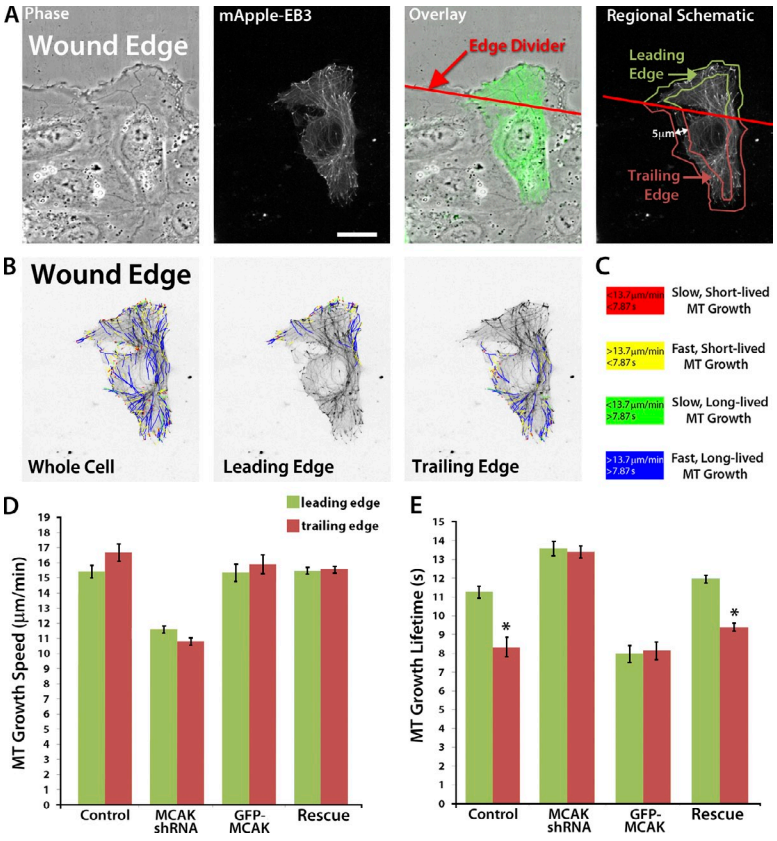

Figure 2. **MCAK limits MT growth in the trailing edge of migrating cells.** (A) Phase-contrast, mApple-EB3, overlay (EB3 shown in green), and schematic depicting the methodology used for defining the leading and trailing edge regions of HUVECs at the edge of a monolayer wound. The line labeled "edge divider" was placed along the edge of the wound to maximize its intersection with distal-most cell–cell junctions as determined from a larger field-of-view image. The edge of the wound faces up. (B) Example of overlays of MT growth tracks from 2-min time-lapse videos of mApple-EB3 (2-s intervals) from plusTipTracker software of tracks for the whole cell and subpopulations of tracks from the leading or trailing edge regions of the cell depicted in A. (C) MT growth tracks in B are color coded according to their growth speed and lifetime. (D and E), Comparison of mean MT growth speeds (D) and mean MT growth excursion lifetimes (E) within the leading and trailing edges of wound-edge HUVECs. Bar, 10 μm. *, $P < 0.001$. Error bars show ± standard error.

knockdown slowed MT growth speed and increased MT growth lifetime, whereas MCAK overexpression reduced MT growth lifetime. Rescue of MCAK knockdown returned both MT growth speed and lifetime to control levels (Fig. 1, J and K). Together, these results indicate that MCAK tracks with growing MT plus ends and limits the lifetime of MT growth excursions in HUVECs.

To determine the role of MCAK-mediated regulation of MTs in HUVEC function, we assayed branching morphogenesis in HUVECs cultured on collagen coupled to soft (0.7 kPa) polyacrylamide substrates to promote cell branching (Fischer et al., 2009) and directed cell migration in a wound-healing assay. We coexpressed an mApple volume marker along with either BFP-tagged control shRNA, MCAK shRNA, GFP-MCAK, or Rescue (Fig. 1 L). Quantification of HUVEC branching showed that both MCAK knockdown and overexpression significantly reduced the number of branches per cell (Fig. 1 N), but did not significantly affect branch length (Fig. 1 O). Expression of GFP-MCAK in cells depleted of endogenous MCAK rescued HUVEC branching (Fig. 1 N) and similarly did not influence branch length (Fig. 1 O). Analysis of HUVEC migration in a wound-healing assay (Fig. 1 M) revealed that either MCAK-shRNA or expression of GFP-MCAK significantly impaired directional migration and that the effects of MCAK knockdown on migration were reversed by expression of GFP-MCAK (Fig. 1 P). Together, these results suggest that a balance of MCAK expression is required to fine tune MT assembly dynamics to promote HUVEC branching morphogenesis and directional migration.

MCAK limits MT growth in the trailing edge of migrating cells

Because MT assembly dynamics are polarized in the cell during EC branching (Myers et al., 2011) and directional migration in other cell types (Waterman-Storer et al., 1999; Wittmann et al., 2003), we hypothesized that MCAK may differentially regulate MT dynamics in the leading versus trailing edges of migrating HUVECs. Examination of GFP-MCAK localization in the leading and trailing edges of HUVECs at the edge of a monolayer wound revealed no bias between MCAK localization and leading edge or trailing edge MTs (Fig. 1 B). Unfortunately, all available anti-MCAK antibodies used for immunofluorescence stained HUVECs with very high levels of background, rendering localization of the endogenous protein untenable.

Although MCAK localization was not polarized, this does not rule out the possibility that its activity may regionally regulate MT dynamics. To test this, we compared MT growth dynamics in the leading and trailing edges of wound-edge HUVECs with altered levels of MCAK expression. HUVECs were transfected with mApple-EB3 together with control shRNA, MCAK shRNA, GFP-MCAK, or MCAK shRNA together with GFP-MCAK (Rescue). To first validate that MT growth is regionally regulated during HUVEC migration, we used automated tracking of mApple-EB3 and compared MT dynamics in the leading versus trailing edges of migrating HUVECs (Fig. 2, A–C). This showed that, in control cells, MT growth speed was similar throughout the cell; however, MTs underwent longer-lived growth excursions in the leading edge compared with the trailing edge, similar to other cell types (Fig. 2, D and E;

Wittmann et al., 2003). Analysis of MT growth tracks showed that the effects of MCAK manipulations did not regionally affect MT growth speed (Fig. 2 D). However, comparison of MT growth lifetimes revealed that when MCAK expression was reduced by shRNA, MTs specifically increased their growth lifetime in the cell rear, thus homogenizing regional differences in MT growth lifetimes such that they were long lived throughout the cell (Fig. 2 E). In contrast, overexpression of GFP-MCAK significantly reduced MT growth lifetime specifically at the leading edge, resulting in a loss of regional difference in MT growth lifetime between leading and trailing edges. Additionally, the loss of regional difference of MT growth dynamics that resulted from shRNA-mediated knockdown of MCAK was rescued by expression of GFP-MCAK (Rescue; Fig. 2 E). These results show that MCAK maintains polarization of short-lived MT growth in the cell rear and long-lived MT growth toward the leading edge of directionally migrating cells, and suggests that this may be achieved by enhancing MT assembly specifically in the leading edge by local inactivation of MCAK activity.

Active Aurora A associates with MCAK on MTs

Aurora family kinases, Aurora A and B, phosphorylate MCAK to inhibit its depolymerase activity (Andrews et al., 2004; Lan et al., 2004; Ohi et al., 2004; Knowlton et al., 2006; Zhang et al., 2007, 2008; Tanenbaum et al., 2011). Although localization of Aurora B is restricted to the nucleus during interphase (Andrews et al., 2004; Lan et al., 2004; Ohi et al., 2004; Rannou et al., 2008), Aurora A is present in the interphase cytoplasm of human epithelial cells (Rannou et al., 2008). To determine if Aurora A may contribute to regional regulation of MCAK in HUVECs during directed migration, we first examined its localization. Live-cell imaging of cells cotransfected with mEmerald (Em) fluorescent protein fused to Aurora A (Em–Aurora A) and mApple-EB3 showed that, similar to MCAK, Em–Aurora A tracked with growing MT plus ends and was also localized along the length of subsets of MTs (Video 2). To determine if Aurora A showed a polarized localization in association with MCAK or MTs, cells in a wound-healing assay were cotransfected with low levels of Em–Aurora A together with mCherry-MCAK or mApple fusions of EB3 or tubulin (Fig. 3, A–C). Colocalization was then analyzed at the leading and trailing edges of wound-edge HUVECs. Quantification of the fraction of Aurora A that was colocalized with EB3 or tubulin showed a bias in colocalization of Aurora A with MTs and growing plus ends in the leading compared with the trailing cell edge. In addition, although only a small proportion of Aurora A was colocalized with MCAK (~12%), there was more than four times more Aurora A–MCAK colocalization in the leading than the trailing edge (Fig. 3 D).

To determine the location of Aurora A activity in the cell, we used an antibody that recognizes the activated form of Aurora A that is phosphorylated on threonine 288 (pT288–Aurora A; Littlepage et al., 2002). This showed that a population of endogenous, phosphorylated Aurora A associated specifically with MTs extending into leading edge protrusions (Fig. 3 E). Overexpression of Em–Aurora A promoted increased levels of active (pT288) Aurora A at the leading edge (Fig. 3 F), whereas pharmacological inhibition of Aurora A (40 nM Aurora A Inhibitor) eliminated leading edge pT288–Aurora A labeling of MTs (Fig. 3 G). MCAK localization did not show bias in control, Aurora A–inhibited, or Aurora A–expressing cells (Fig. 4, A–C), suggesting that activated Aurora A localizes with MCAK on leading edge MTs in migrating HUVECs where it may locally regulate MCAK activity.

To determine if Aurora A activity affects its association with MCAK, we performed coimmunoprecipitations. Cells were transfected with GFP–Aurora A or, as a control, were transfected with a GFP-tagged focal adhesion protein, Zyxin (GFP-Zyxin), and precipitated with anti-GFP antibodies followed by Western blot analysis with antibodies to MCAK (Fig. 4 D). This showed that GFP–Aurora A coprecipitated MCAK from the cytoplasmic fraction of HUVEC lysates, whereas a similar immunoprecipitation of GFP-Zyxin did not coprecipitate MCAK. Conversely, immunoprecipitation of endogenous MCAK in untransfected cells coprecipitated the active form of Aurora A (Fig. 4 E), whereas control immunoprecipitation of GAPDH did not. Association of Aurora A with MCAK was dependent on Aurora A activity, as treatment of HUVECs with 40 nM Aurora A inhibitor (Fig. 4 E) substantially reduced their coprecipitation, suggesting that MCAK predominantly interacts with the activated form of Aurora A. Thus, Aurora A associates with MCAK in an activity-dependent manner. Altogether, these results suggest that activated Aurora A associates with MCAK on MTs in the leading edge of migrating HUVECs.

Aurora A rescues MCAK overexpression and promotes long-lived MT growth at the leading edge

We next sought to determine if Aurora A activity regulates MT assembly dynamics through MCAK. Because investigations of MCAK effects on MT growth dynamics (Figs. 1 and 2) revealed significant differences specifically in the spatial regulation of MT growth lifetimes, we focused our analysis on comparisons of MT growth lifetimes for the remainder of our studies. Complete analysis of MT growth speed and MT growth lifetimes can be found in Figs. S1 and S2. Analysis of mApple-EB3 tracks in image series of cells overexpressing Em–Aurora A, cells treated with Aurora A inhibitor, MCAK knockdown cells treated with Aurora A inhibitor, or cells coexpressing MCAK and Em–Aurora A (Fig. 5, A–D) revealed that expression of Aurora A promoted long-lived MT growth excursions (Fig. 5 A, green and blue tracks). In contrast, pharmacological inhibition of Aurora A in control cells had little effect on MT growth lifetime (Fig. 5, B and H). However, inhibition of Aurora A in cells depleted of endogenous MCAK (Fig. 5, C and H) displayed MT growth lifetimes similar to either MCAK shRNA alone or Em–Aurora A expression alone (see Fig. 1, F and K; or Fig. S1). Additionally, coexpression of MCAK together with Em–Aurora A (Fig. 5, D and H) resulted in an increase in MT growth lifetimes that was similar to expression of Em–Aurora A or MCAK shRNA alone (see Fig. 1, F and K; or Fig. S1). Thus, Aurora A overexpression can promote long-lived MT growth, Aurora A effects on MT growth lifetimes require MCAK to be

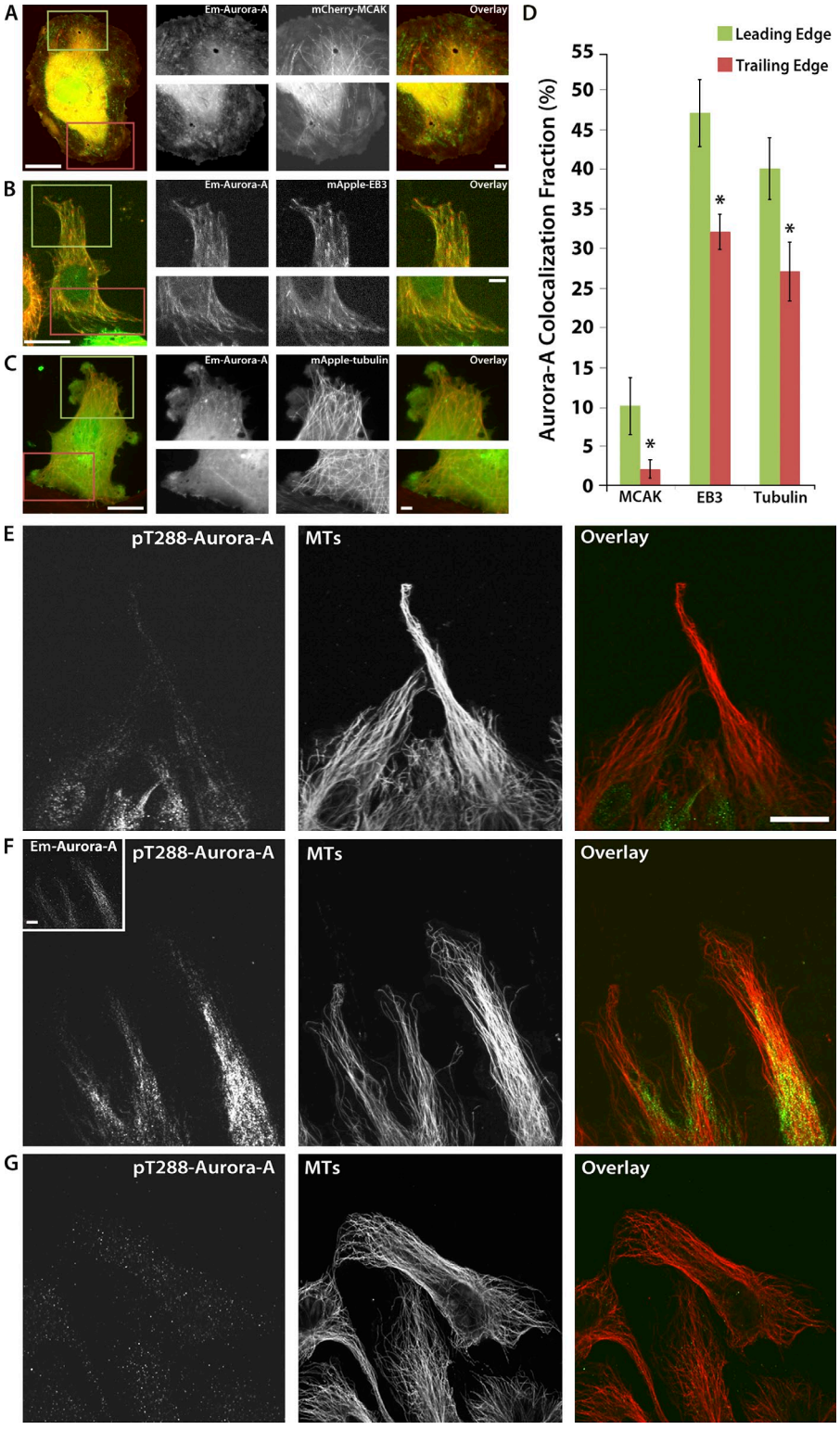

Figure 3. **Active Aurora A associates with MCAK on MTs.** (A–C) Images showing the whole cell (left) and zoomed regions of the leading (green boxes and top right row) and trailing edges (red boxes and bottom right row) of HUVECs at the edge of a monolayer wound expressing Em–Aurora A and either mCherry-MCAK (A), mApple-EB3 (B), or mApple-tubulin (C; see also Video 2). In all panels, the wound edge faces up. (D) Quantification of the fraction of Em–Aurora A that colocalizes with MCAK, EB3, or tubulin under experimental conditions shown in A–C. (E–G) Immunolocalization of pT288–Aurora A and MTs in control (E), Em–Aurora A–expressing (F; inset, Em–Aurora A localization), and wound-edge HUVECs treated with an Aurora A inhibitor (G). Bars: (main) 10 µm; (zoomed) 2 µm; (F, inset) 10 µm. *, $P < 0.05$. Error bars show ± standard deviation.

present in cells, and Aurora A is sufficient to rescue the effects of MCAK expression on MT growth dynamics, as would be expected for a negative regulator of MCAK activity.

We then determined if Aurora A regulates polarized MT growth dynamics via MCAK in migrating cells. Tracking fluorescently labeled EB3 in the leading and trailing edges of wound-edge HUVECs showed that, compared with control, overexpression of Em–Aurora A increased MT growth lifetime in both the leading and trailing edges. In contrast, pharmacological inhibition of Aurora A activity resulted in reduced MT growth lifetime in the leading edge and increased MT growth lifetime in the trailing edge, and the effect of Aurora A inhibition on regional MT growth lifetimes was dependent on the presence of endogenous MCAK (Fig. 5 I). Thus, Aurora A promotes

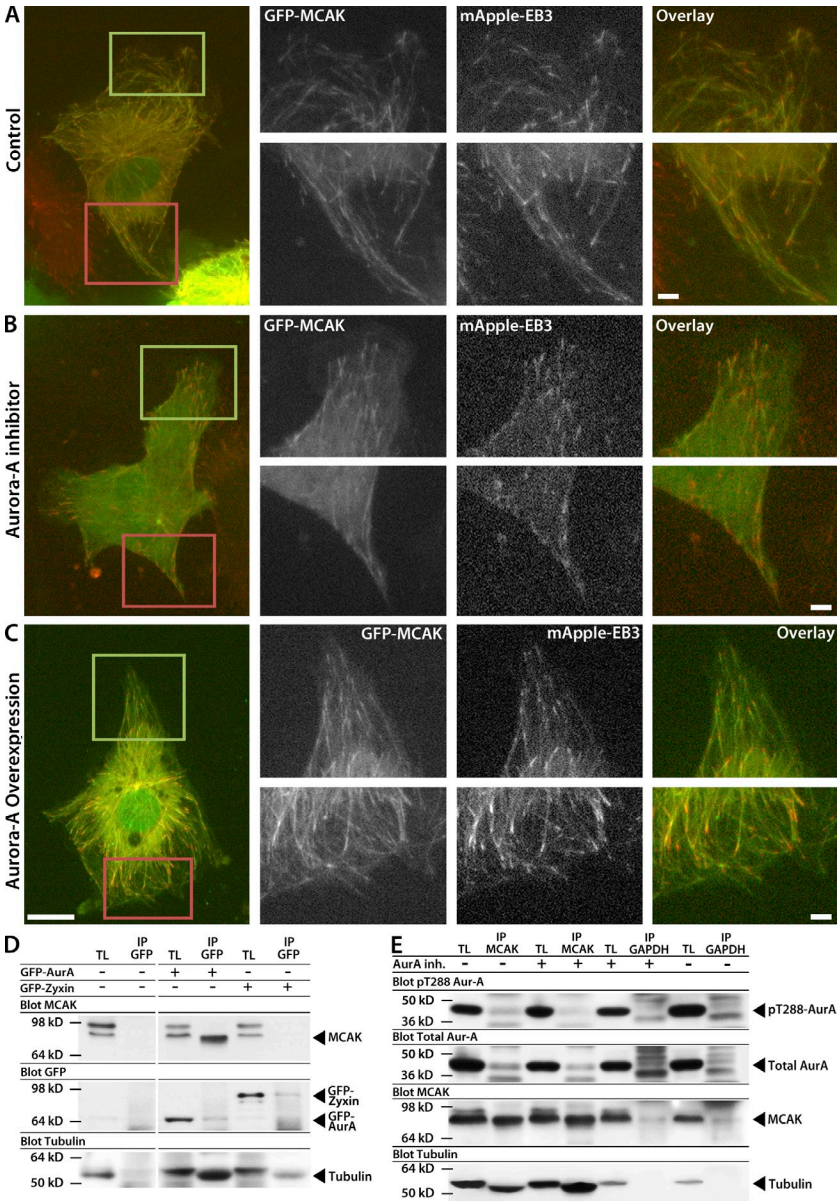

Figure 4. **Aurora A activity is required for association with MCAK but does not affect MCAK localization to growing MT plus ends.** (A–C) Images showing the whole cell (left) and zoomed regions of the leading (green boxes and top right row) and trailing edges (red boxes and bottom right row) of HUVECs at the edge of a monolayer wound coexpressing mApple-EB3 and low levels of GFP-MCAK. The wound edge faces up. Fluorescent images reveal MCAK localization to growing MT plus ends in HUVECs in untreated control (A), treated with 40 nM Aurora A inhibitor (B), or overexpressing Aurora A (C). (D) Immunoprecipitation from HUVEC lysates with anti-GFP antibodies in HUVECs in the absence (−) or presence (+) of GFP–Aurora A or GFP-Zyxin expression and Western blot with anti-MCAK (top) or anti-GFP antibodies (bottom). Note that MCAK appears as a doublet in HUVEC lysates, and that the lower molecular mass form exclusively coimmunoprecipitates with Aurora A. (E) Immunoprecipitation with anti-MCAK or anti-GAPDH antibodies from HUVEC cell lysates prepared in the absence (−) or presence (+) of 40 nM Aurora A inhibitor and Western blot with anti–pT288–Aurora A, anti–Aurora A, and anti-MCAK antibodies. Western blot for tubulin shows coprecipitation with GFP–Aurora A (D) and with MCAK (E). IP, immunoprecipitate; TL, total lysate. Bars: (main) 10 µm; (zoomed) 2 µm.

polarized growth of MTs in a MCAK-dependent manner by limiting MT growth lifetime in the rear and promoting longer-lived MT growth in the leading edge. Coexpression of Aurora A and MCAK increased MT growth lifetime specifically in the cell rear, similar to either Aurora A or MCAK shRNA expression alone (Fig. 5 I and Fig. 2 E). Thus, Aurora A activity is required to promote polarized MT growth in migrating HUVECs and is also able to rescue the effects of MCAK overexpression on MT growth lifetimes by promoting growth in the leading edge.

MCAK depolymerase activity is inhibited by Aurora family kinases via phosphorylation at several distinct serine residues during mitosis (Lan et al., 2004; Ohi et al., 2004; Zhang et al., 2007, 2008), but the site responsible for its regulation during cell migration is not known. To determine which Aurora A phosphorylation site in MCAK is required for its inhibition at the leading edge of polarized HUVECs, we evaluated MT growth dynamics in wound-edge HUVECs expressing fluorescent EB3, depleted of endogenous MCAK, and rescued with MCAK mutants altered in known Aurora kinase phosphorylation sites. We used nonphosphorylatable (serine to alanine) and phosphomimic (serine to glutamic acid) MCAK, mutated in multiple known Aurora phosphorylation sites (serines 92, 106, 108, 112, and 196 [AAAAA MCAK and EEEEE MCAK]), as well as in two specific sites—serine 196 (S196A MCAK and S196E MCAK) and serine 719 (S719A MCAK and S719E MCAK). Analysis revealed that expression of either the AAAAA MCAK or S196A MCAK nonphosphorylatable mutants in MCAK knockdown cells was able to rescue the increase in MT growth lifetime induced by MCAK knockdown alone, reducing MT growth lifetime to levels similar to untransfected controls or Aurora A–inhibited HUVECs and regionally homogenizing MT growth lifetime (Figs. 5 [H and I], 1 K, and S1). In contrast, rescue with either the phosphomimic EEEEE MCAK or S196E MCAK mutants had similar effects on MT growth lifetime as MCAK knockdown or Aurora A overexpression (Figs. 5 H and S1). Additionally, rescue of MCAK knockdown

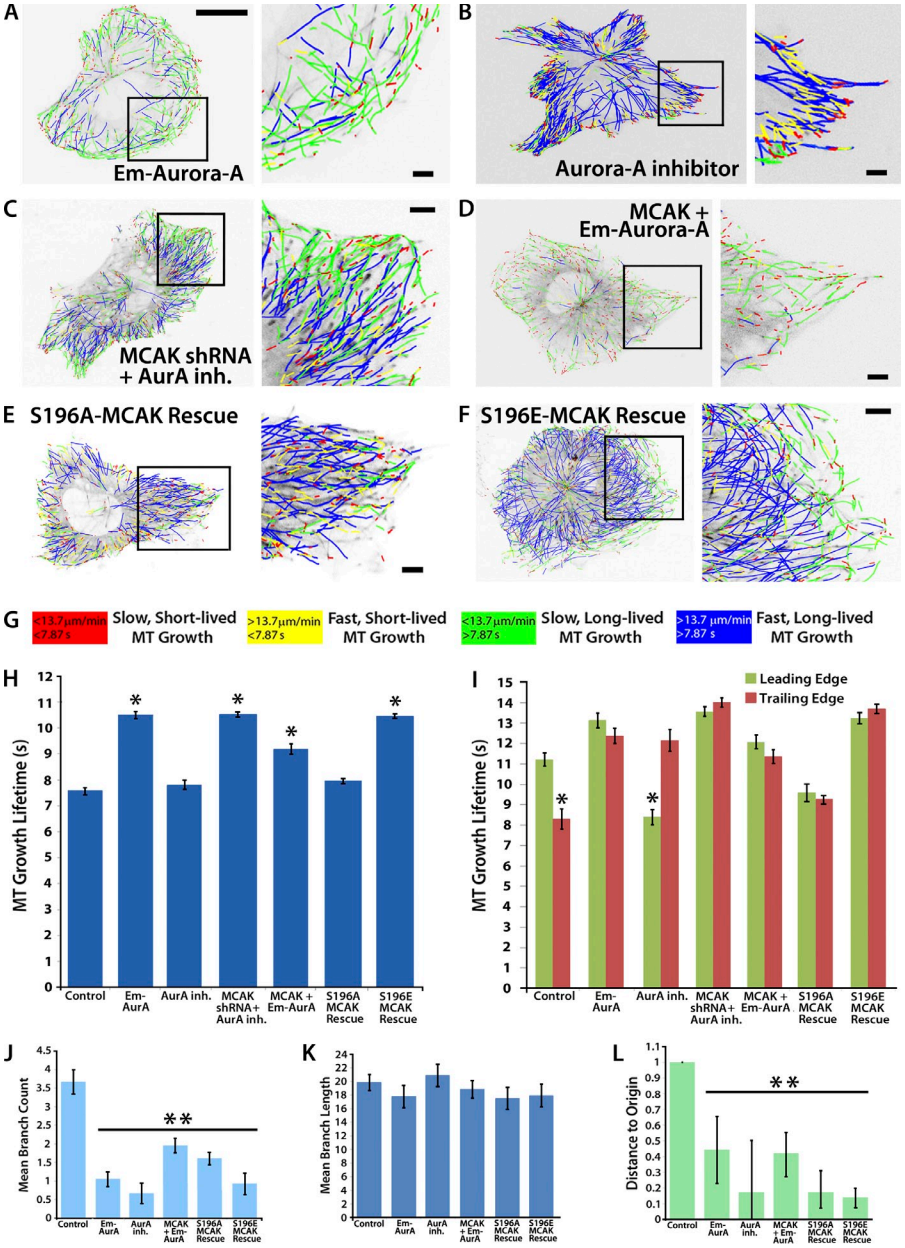

Figure 5. **Aurora A rescues MCAK overexpression and promotes long-lived MT growth at the leading edge.** (A–F) Overlays of MT growth tracks from 2-min time-lapse videos of mApple-EB3 (2-s intervals) from plusTipTracker software in whole cells (left), and zoom of black-boxed regions (right) of HUVECs overexpressing Em–Aurora A in cells treated with 40 nM Aurora A inhibitor, in MCAK knockdown cells treated with Aurora A inhibitor, in cells cooverexpressing mCherry-MCAK and Em–Aurora A, or in shRNA-treated HUVECs rescued with MCAK S196A or S196E mutant constructs. MT tracks are color coded according to their growth speed and lifetime (color scheme in G). (H–L) Comparison of parameters for MT and cell behavior for the treatments of HUVECs described in A–F. Comparison of mean MT growth excursion lifetimes in whole cells (H) and within the leading and trailing edges of wound-edge HUVECs (I). Quantification of branch number (J) and length (K) in HUVECs cultured on fibronectin-coupled 0.7-kPa polyacrylamide substrates to promote branching morphologies. (L) Quantification of directional HUVEC migration in wound-edge migration assay. Bars: (main) 10 µm; (zoomed) 2 µm. *, $P < 0.001$; **, $P < 0.05$. Error bars show ± standard error in H and I and ± standard deviation in J–L.

with either S719A or S719E MCAK blocked the increase in growth lifetime induced by MCAK depletion (Fig. S1), indicating that phosphorylation on this site does not regulate MCAK activity. These results show that the S196A-MCAK mutant inhibits MT assembly, whereas the S196E-MCAK mutant promotes MT assembly, suggesting that phosphorylation on S196 is specifically required for down-regulation of MCAK activity to promote MT growth.

To determine the role of Aurora A in HUVEC function, we assayed HUVEC branching morphogenesis and directed migration in cells with altered Aurora A level or activity. Quantification of HUVEC branching on soft polyacrylamide ECMs showed that either Aurora A overexpression or pharmacological inhibition significantly reduced cell branching (Fig. 5 J), but did not affect branch length (Fig. 5 K). Analysis of HUVEC migration in a wound-healing assay revealed that, similar to the result of impaired EC branching, Aurora A overexpression or inhibition significantly impaired directional migration (Fig. 5 L). Coexpression of Aurora A with MCAK increased both branch number and directional migration, but did not modify these parameters back to control levels, suggesting that a regional balance of Aurora A activity may be required to promote HUVEC branching morphogenesis and directed migration. Additionally, MCAK rescue experiments revealed that neither the S196A nor the S196E MCAK mutant was able to rescue EC branching and migration parameters (Fig. 5, J–L). This result was unlike the wild-type MCAK rescue, which was sufficient to rescue EC branching and migration parameters similar to control measurements (see Fig. 1, L–P). Together, these results further support the conclusion that a regional balance of MCAK regulation by Aurora A activity are required to promote HUVEC branching morphogenesis and directed migration.

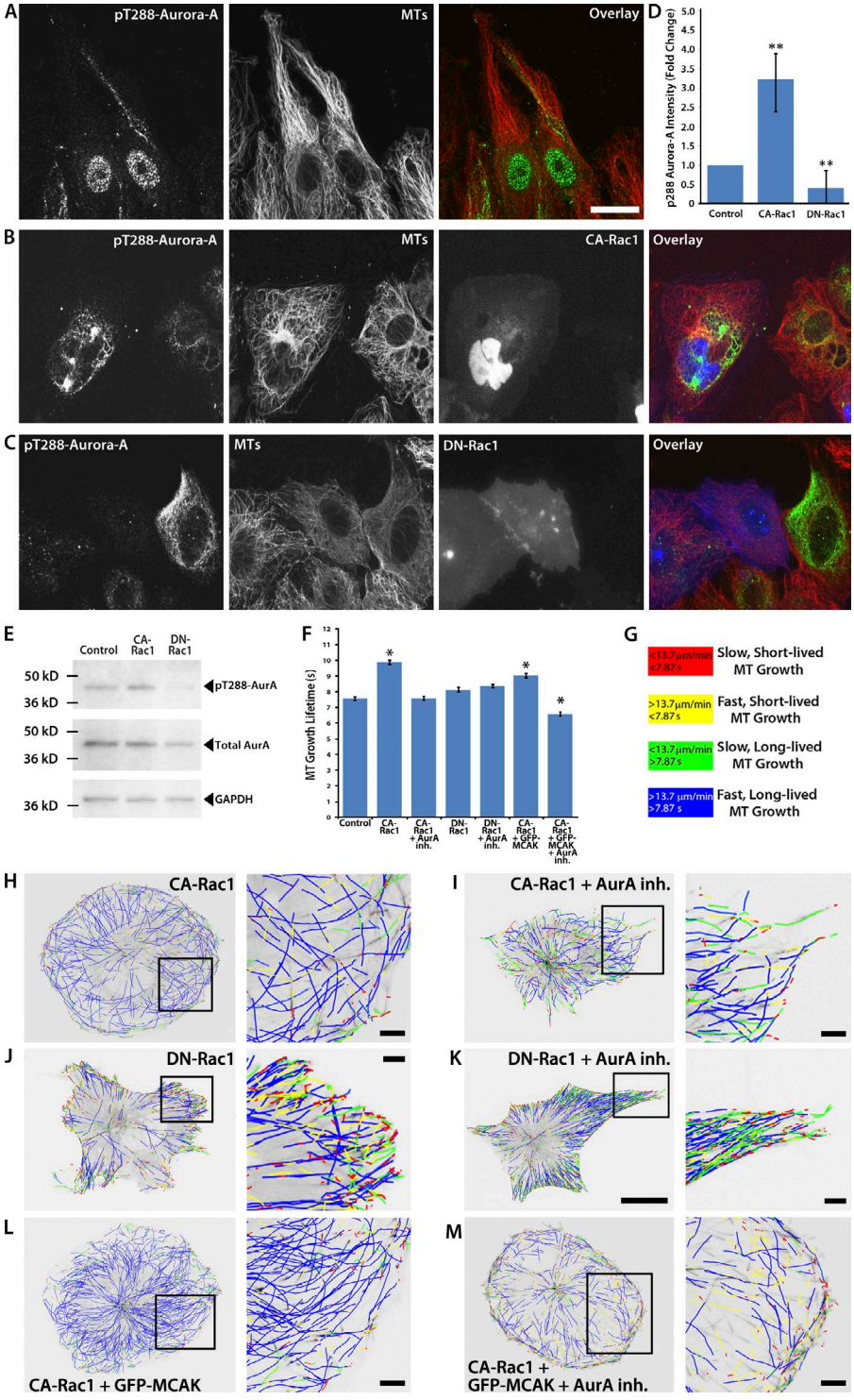

Figure 6. **Aurora A regulates MT dynamics in response to Rac1 activity.** (A–C) Immunolocalization of pT288–Aurora A and MTs in untransfected control HUVECs (A) or HUVECs expressing BFP-tagged CA-Rac1 (B) or DN-Rac1 (C) at the edge of a monolayer wound. The wound edge faces up. (D) Quantification of fluorescence intensity measurements of pT288–Aurora A in wound-edge HUVECs under the conditions described in A–C. (E) Western blot for pT288–Aurora A in lysates of untransfected control HUVECs (control) or HUVECs expressing CA-Rac1 or DN-Rac1. Lysates were also probed for total Aurora A, and GAPDH is shown as a loading control. (F) Comparison of mean MT growth lifetimes measured from 2-min time-lapse videos of mApple-EB3 using plusTipTracker software in HUVECs expressing mApple-EB3 (control) or HUVECs coexpressing mApple-EB3 and CA-Rac1 or DN-Rac1 in the presence or absence of 40 nM Aurora A inhibitor, or coexpressing mApple-EB3 and CA-Rac1 or DN-Rac1 and GFP-MCAK in the presence or absence of 40 nM Aurora A inhibitor. (G–M) MTs are color coded according to their growth speed and lifetime (color scheme in G). (H–M) MT growth tracks from 2-min time-lapse videos of mApple-EB3 (2-s intervals) overlaid on images of whole HUVECs (left) and zoom of black-boxed regions (right) of HUVECs, treated as described. Bars: (main) 10 µm; (zoomed) 2 µm. *, $P < 0.001$; **, $P < 0.05$. Error bars show ± standard error in F and ± standard deviation in D.

Aurora A regulates MT dynamics in response to Rac1 activity

The small GTPase Rac1 promotes leading edge MT growth in migrating cells (Wittmann et al., 2003; Gundersen et al., 2005). To investigate whether Rac1 signaling acts via Aurora A in regulation of MT growth dynamics in HUVECs, we first examined the effects of manipulating Rac1 activity on the phosphorylation of Aurora A. Cells were transfected with either constitutively active (CA) or dominant-negative (DN) mutants of Rac1 and Aurora A phosphorylation (pT288) was analyzed by immunofluorescence (Fig. 6, A–C). Quantification of images showed that pT288–Aurora A was enhanced 312 ± 64% by CA-Rac1 and reduced 220 ± 87% by DN-Rac1 compared with control (Fig. 6 D). A similar trend was confirmed by immunoblotting lysates of cells expressing Rac1 mutants for pT288–Aurora A. This revealed a 65 ± 4% increase and a 61 ± 6% decrease in Aurora A phosphorylation in cells expressing CA-Rac1 and DN-Rac1 compared with control, respectively (Fig. 6 E). These

results indicate that activated Rac1 promotes downstream phosphorylation and activation of Aurora A.

To determine if Rac1 regulation of MT growth is mediated through Aurora A, we tracked mApple-EB3 dynamics in cells with perturbed Rac1 and Aurora A function. Analysis of MT growth tracks in CA-Rac1– versus DN-Rac1–expressing cells (Fig. 6, F–M) revealed that CA-Rac1 promoted long-lived MT growth compared with controls, similar to observations in other cell types (Wittmann et al., 2003) and similar to the effects of Aurora A overexpression or MCAK shRNA (see Figs. 1, 3, and S1). Pharmacologic inhibition of Aurora A in cells expressing CA-Rac1 reduced MT growth lifetimes to control levels (Fig. 6, F and I). Expression of DN-Rac1 alone or in combination with Aurora A inhibitor had no effect on MT growth lifetimes (Fig. 6, F, J, and K). Expression of CA-Rac1 together with GFP-MCAK reverted the effects of MCAK overexpression (Fig. 6, F and L), increasing MT growth lifetimes compared with expression of GFP-MCAK alone (see Figs. 1 and S1) and similar to the effects of CA-Rac1 expression alone, suggesting that the effects of MCAK on MT growth dynamics are regulated by Rac1 activity. To determine if this effect was mediated through Aurora A, we treated cells expressing CA-Rac1 and GFP-MCAK with Aurora A inhibitor (Fig. 6 M). Here, Aurora A inhibition promoted short-lived MT growth excursions, similar to GFP-MCAK expression or Aurora A inhibitor alone (Fig. 6 F and Fig. S1). Together, these results suggest that Rac1 promotes downstream phosphorylation and activation of Aurora A to inhibit the effects of MCAK on MT growth dynamics, resulting in the promotion of long-lived MT growth.

Rac1 promotes long-lived leading edge MT growth excursions in an Aurora A– and MCAK-dependent manner

To determine how the Rac1–Aurora A–MCAK signaling pathway regulates MT growth dynamics in polarized cell migration, we first evaluated how Rac1 activity affects the colocalization of Aurora A with MCAK, EB3, or MTs in HUVECs migrating in a wound-healing assay (Fig. 7, A–F). Cells were cotransfected with Em–Aurora A together with mCherry-MCAK, mApple-EB3, or mApple-tubulin, along with BFP-tagged CA-Rac1 (Fig. 7, A–C) or DN-Rac1 (Fig. 7, D–F), and colocalization in the leading and trailing edges were determined. Quantification of the fraction of Aurora A that was colocalized with EB3 or tubulin showed that CA-Rac1 promoted Aurora A colocalization specifically with MTs in the leading edge, whereas DN-Rac1 decreased their colocalization, independent of subcellular location (Fig. 7, G–I; and Videos 3 and 4). Furthermore, CA-Rac1 promoted and DN-Rac1 inhibited Aurora A–MCAK colocalization specifically in the leading edge (Fig. 7 G). These results suggest that active Rac1 promotes Aurora A association with MCAK on MTs and that in polarized migrating cells this preferentially occurs in the leading edge.

To determine if Rac1 regulates polarized MT growth dynamics through Aurora A in migrating cells, we performed automated tracking of images of fluorescently labeled EB3 in the leading and trailing edges of wound-edge HUVECs in which Rac1 and Aurora A activity were perturbed. This showed that compared with controls, CA-Rac1 specifically increased MT growth lifetime in the trailing edge (Fig. 7 J), similar to effects of MCAK knockdown or Aurora A overexpression (see Figs. 2 E and 5 I, or Fig. S2). Inhibition of Aurora A kinase activity in cells expressing CA-Rac1 decreased MT growth lifetime specifically within the leading edge compared with the effects of CA-Rac1 alone (Fig. 7 J), mimicking the effects of Aurora A inhibition alone or MCAK overexpression (see Figs. 2 E and 5 I, or Fig. S2). In contrast, expression of DN-Rac1 specifically decreased growth lifetime in the leading edge and increased growth lifetime in the trailing edge, whereas coexpression of CA-Rac1 and MCAK specifically increased MT growth lifetime in the cell rear, similar to effects of CA-Rac1 or MCAK shRNA alone. Similarly, Aurora A inhibition promoted long-lived MT growth in the trailing edge of wound-edge HUVECs coexpressing CA-Rac1 and GFP-MCAK, similar to the effects of MCAK alone (see Figs. 2 E or S2). Together, these results suggest that Rac1 activation in the leading cell edge promotes local Aurora A association with MCAK on MTs to promote long-lived MT growth at the leading edge of polarized HUVECs.

To investigate whether Rac1 signaling through Aurora A mediates HUVEC branching morphogenesis, we analyzed branching in HUVECs cultured on soft (0.7 kPa) polyacrylamide substrates to promote cell branching when Rac1 and Aurora A function was perturbed. This showed that, compared with control, CA-Rac1 reduced both HUVEC branch number and branch length, whereas DN-Rac1 had no effect (Fig. 7, K and L), suggesting that Rac1 is a negative regulator of EC branching. Combining Rac1 mutants with Aurora A kinase inhibition showed that Aurora A activity is required for HUVEC branching, independent of the activity state of Rac1. In addition, inhibition of Aurora A in HUVECs coexpressing CA-Rac1 and GFP-MCAK could not rescue branch count (Fig. 7 K) or directional migration (Fig. 7 M), suggesting that a fine balance of MT growth dynamics regulation is critical to EC branching and migration. Together, these results suggest that Aurora A acts downstream of Rac1 to regulate HUVEC branching morphogenesis.

Discussion

Regulation of MT growth dynamics is a mechanism used by cells to control their cell morphology dynamically and with localized specificity (Schulze and Kirschner, 1988; Wadsworth, 1999; Akhmanova et al., 2001; van der Vaart et al., 2012). This idea is intuitive and well established, but only in recent years have the analytical tools become available to allow for high volume, quantitative investigations of regional regulation of MT growth dynamics (Matov et al., 2010; Applegate et al., 2011; Myers et al., 2011; Nishimura et al., 2012). Here, we tested the hypothesis that MCAK, a mitotic molecular motor protein that catalytically promotes MT depolymerization, contributes to the regional regulation of MT growth during interphase to guide EC branching morphology and wound-edge migration. Our results suggest that MCAK-mediated regulation of MT growth dynamics is critical to EC control of branching morphology and is similarly critical to EC directional migration. This conclusion stems from a loss of polarized MT growth that is required for

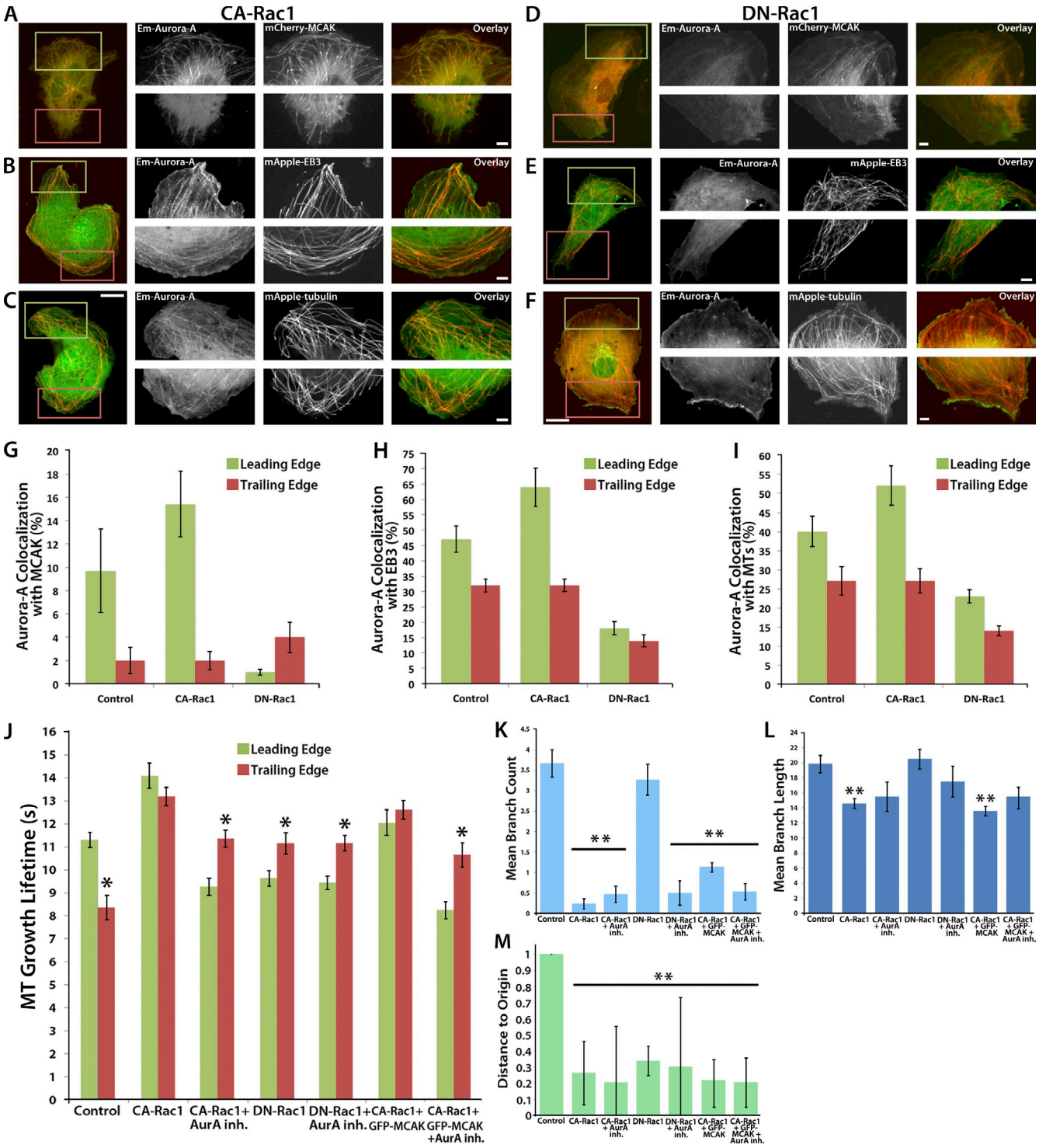

Figure 7. **Rac1 promotes long-lived leading edge MT growth excursions in an Aurora A– and MCAK-dependent manner.** (A–F) Images showing the whole cell (left) and zoomed regions of the leading (green boxes and top right row) and trailing (red boxes and bottom right row) edges of HUVECs at the edge of a monolayer wound that were coexpressing either CA-Rac1 (A–C) or DN-Rac1 (D–F) together with Em–Aurora A and either mCherry-MCAK (A and D), mApple-EB3 (B and E), or mApple-tubulin (C and F; see also Videos 3 and 4). The wound edge faces up. (G–I) Quantification and comparison of the fraction of Em–Aurora A that colocalized with MCAK (G), EB3 (H), or tubulin (I) in control, CA-Rac1, or DN-Rac1–expressing HUVECs. (J) Comparison of mean MT growth lifetimes measured from 2-min time-lapse videos of mApple-EB3 using plusTipTracker software in the leading and trailing edges of wound-edge HUVECs expressing mApple-EB3 (control) or HUVECs coexpressing mApple-EB3 and CA-Rac1 or DN-Rac1 in the presence or absence of 40 nM Aurora A inhibitor, or coexpressing mApple-EB3 and CA-Rac1 or DN-Rac1 and GFP-MCAK in the presence or absence of 40 nM Aurora A inhibitor. Quantification of branch number (K) and length (L) in HUVECs cultured on fibronectin-coupled 0.7-kPa polyacrylamide substrates to promote branching morphologies. (M) Quantification of directional HUVEC migration in wound-edge migration assay. Bars: (main) 10 µm; (zoomed) 2 µm. *, $P < 0.001$; **, $P < 0.05$. Error bars show ± standard deviation in G–I and K–M and ± standard error in J.

the formation of a polarized EC morphology and the resulting inhibition of directional cell migration. Our results also suggest that additional MAPs capable of acting with regional specificity must contribute to fine tuning the regulation of EC MT dynamics to drive productive and polarized EC migration (van der Vaart et al., 2009).

Our findings demonstrate three major points defining MCAK-mediated regulation of EC MTs. First, wound-edge ECs regionally inhibit MCAK's MT-depolymerizing activity to promote MT growth at the leading edge, whereas its unregulated activity in the cell rear promotes reduced MT growth at the trailing edge of the cell. This feature is highlighted by the fact that MCAK tracks with growing, EB3-labeled MT plus ends throughout the cell, yet MCAK's effects of limiting MT growth are specifically focused within the trailing edge of ECs. The results of both our MCAK knockdown and overexpression studies support the results of mitotic studies of MCAK (Maney et al., 1998; Rizk et al., 2009), showing that the primary function of MCAK is to promote fast and short-lived (i.e., dynamic) MT growth. Our results support a mechanism through which the regulation of MCAK's activity as a MT depolymerizing enzyme, not MCAK's localization to MTs, enables the differential control of MT stability in polarized, migrating ECs. However, given that our method is limited to the analysis of only MT growth parameters, it is not known if MT shortening rate, rescue frequency, or pause time may be regulated by MCAK in HUVECs.

Second, we find that regional inhibition of MCAK within the cytoplasm of ECs is achieved through the phosphorylation of MCAK at Serine 196 and that this is promoted by Aurora A kinase. This inhibition involves a physical interaction between MCAK and the active (pT288)–Aurora A, which preferentially localizes to subsets of MTs at the leading edge of wound-edge HUVECs. Although colocalization of Aurora A and MCAK is heightened specifically within the leading edge of polarized wound-edge HUVECs, our results suggest that the regulation of MCAK's MT-depolymerizing activity depends on the kinase activity of Aurora A. Furthermore, we find that the addition of an Aurora A–specific inhibitor results in reduced MT growth lifetimes specifically within the leading edge of polarized HUVECs and that this effect is MCAK dependent. Together, these findings suggest that MCAK normally functions as an active MT-depolymerizing molecular motor in the cytoplasm of interphase cells. In polarized, migrating HUVECs, selective inhibition of MCAK depolymerase activity is achieved in the leading edge where it colocalizes with Aurora A kinase, whose activation is regionally regulated via phosphorylation. Thus, proper control of the levels of active Aurora A kinase within interphase ECs defines regional control of MCAK activity, and thereby controls regional regulation of MT depolymerization, by promoting MT stabilization at the leading edge of polarized wound-edge HUVECs.

Third, our results identify that Aurora A activation is controlled via signaling from the Rho GTPase, Rac1. Expression of the CA-Rac1 results in enhanced overall levels of the pT288–Aurora A, whereas the DN-Rac1 inhibits Aurora A phosphorylation and reduces leading edge MT stabilization, likely through Aurora A's down-regulation of MCAK. This supports the notion that Rac1 acts as a master controller of MAPS that regulate MT growth in the leading edge of migrating cells by down-regulating two MT destabilizers, Op18/stathmin (Wittmann et al., 2004) and MCAK (the present work) and promoting the activity of the MT stabilizer, CLASP (Wittmann and Waterman-Storer, 2005). The intermediaries between Rac1 and these MAPS are not thoroughly fleshed out. A previous investigation supports the involvement of the direct Rac1 effector Pak1 in regulating Op18/stathmin (Wittmann et al., 2004). Whether PAK is involved in the Rac1–Aurora A–MCAK pathway identified here is not clear. Recent studies suggest that MCAK is directly regulated by Pak1 to control MT dynamic instability (Pakala et al., 2012) and that Pak1 is capable of regulating centrosomal Aurora A, although this effect was found to be RhoGTPase independent (Zhao et al., 2005). However, our attempts to measure the effects of Pak1 on Aurora A activity and MT growth dynamics support the notion that Aurora A works through a Pak-1–independent pathway to control interphase MT growth dynamics (unpublished data). These results support the possibility that other Rho family effectors may serve as signaling intermediates to target Aurora A kinase for activation and MCAK for down-regulation.

Together, our results establish a previously undefined signaling pathway that controls EC morphogenesis whereby activation of Rac1 triggers the phosphorylation and activation of Aurora A kinase at the leading edge of wound-edge HUVECs. Activation of Aurora A kinase results in phosphorylation of MCAK at Serine 196, which induces the local inhibition of MCAK-mediated MT disassembly and promotes MT growth specifically at the leading cell edge. Our data suggest that this type of localized regulation is the key step for defining regional differences in MT growth parameters necessary to drive EC branching and polarity as well as to guide directional EC migration. Our findings highlight one pathway used by ECs to fine-tune the control of MT growth dynamics by differentially inhibiting the MT depolymerizing activity of MCAK locally within the cell to regulate EC morphology and angiogenesis. Our findings also suggest that Aurora A inhibitors, a treatment currently under investigation to block cancer cell division, may also contribute to the inhibition of cancer metastasis and tumor angiogenesis.

Materials and methods

Cell culture

Cell culture. HUVECs were cultured and maintained in EBM medium supplemented with EGM-MV Single Quots (Lonza) at 37°C in 5% CO_2. For live imaging, HUVECs were cultured at 50,000 cells/coverslip on 10 µg/ml fibronectin-coated glass coverslips (except for experiments using polyacrylamide substrates) and medium was supplemented with 25 µM Hepes, pH 7.2, and 30 U/ml Oxyrase. For Aurora A inhibition studies, cells were treated with 40 nM Aurora A Inhibitor I (Selleck Chemicals) for 60 min before imaging. Transfection of cDNAs and shRNA was performed using a Nucleofector Device with solution kit V (Lonza), setting A-034, and experiments were performed 6–10 h later to allow time for protein expression and/or shRNA knockdown.

Polyacrylamide substrates. For HUVEC branching studies, flexible polyacrylamide substrates were generated as previously described (Fischer et al., 2012). In brief, 22-mm No. 1.5 coverslips were activated by treatment with 50% 3-aminopropyltrimethyloxysilane and 0.5% glutaraldehyde, and each treatment was followed by extensive double-distilled H_2O washing. Activated coverslips were inverted on a freshly mixed solution of 40% acrylamide and 2% bis-acrylamide to give an adhered polyacrylamide gel with a stiffness of 0.7 kPa. To bind fibronectin, gel

substrates were activated by 2 mM sulfo-SANPAH by exposure to 7,500 J of UV light, rinsed, covalently coupled to 10 µg/ml fibronectin (EMD), incubated for 3 h at 37°C, rinsed three times in PBS, and stored in PBS at 4°C before cell culture.

Expression constructs

Generation of shRNA and cDNA expression constructs. MCAK knockdown experiments were conducted by expressing shRNA under the control of the polymerase-III H1-RNA gene promoter based on the pSuper vector backbone (Brummelkamp et al., 2002). To allow for microscopic identification of shRNA-expressing cells while maintaining the availability of the GFP channel for other fluorescent probes, the pEGFP-C3 sequence (Takara Bio Inc.; Kita et al., 2006) was replaced with the mTagBFP2-C1 sequence (Takara Bio Inc.) to create an H1-mTagBFP cDNA plasmid. To generate MCAK shRNAs against human MCAK (RefSeq accession no. NM_006845) the following oligonucleotides were synthesized and ligated into the H1-mTagBFP cDNA plasmid after restriction enzyme digest with BglII and XhoI: MCAK shRNA forward sequence, 5′-AAGCTCCTGTGAATATACTTTCTTCCTGTCAAAAGTATATTCACAGGAGCTT-3′; control shRNA forward sequence, 5′-GGAATCTCATTCGATGCATACCTTCCTGTCAGTATGCATCGAATGAGATTCC-3′. *Ceanothus griseus* MCAK (RefSeq accession no. NP_001233671.1) cDNAs, labeled with either GFP or mCherry, were obtained from L. Wordeman (University of Washington, Seattle, WA). EGFP–Aurora A was obtained from E. Nigg (University of Basel, Basel, Switzerland) and modified as follows. The Em–Aurora A fusion was assembled using an advanced EGFP variant with several mutations designed to enhance brightness and folding efficiency (Teerawanichpan et al., 2007; Em: wild-type GFP + F64L, S65T, S72A, N149K, M153T, I167T, and A206K). The resulting targeting vectors were used as pilots to demonstrate proper localization of the fusions to their designated subcellular locations. All DNA preparations used a C-terminal vector backbone (Takara Bio Inc.) with a CMV promoter. To construct human Aurora kinase A (RefSeq accession no. NM_198433.1), the following primers were used to amplify aurora kinase A cDNA with the inclusion of a 7–amino acid linker (SGLRSRA) positioned between the targeting Aurora A gene product and the fluorescent protein: AgeI forward sequence, 5′-GCGCTACCGGTCGCCACCATGGTGAGCAAGGGCGAGGAGCTGTTC-3′; BamHI reverse sequence, 5′-CCGGTGGATCCCTAAGACTGTTTGCTAGCTGATTC-3′. This fragment, along with a C1 cloning vector backbone (Takara Bio Inc.), was then digested with AgeI and BamHI, gel purified, and ligated to generate EGFP–Aurora A–C7. The plasmid, along with an Em-C1 cloning vector, was sequentially digested with AgeI and XhoI, gel purified, and ligated to form Em–Aurora A–C7. All DNA used for transfection was prepared using the Plasmid Maxi kit (QIAGEN).

Microscopy and image analysis

Live-cell imaging. All imaging was performed on a spinning disk (Yokagawa CSU-X1; Andor Technology) confocal microscope using a 60× 1.4 NA oil immersion objective lens on a TiE microscope equipped with Perfect Focus System (Nikon) equipped with an electronic shutter (Smart shutter; Sutter Instrument) for transmitted illumination, a linear encoded X and Y, motorized stage (ASI Technologies), and a multi-bandpass dichromatic mirror (Semrock) and bandpass filters (Chroma Technology Corp.) in an electronic filterwheel for selection of GFP or Texas red emission. 561- and 488-nm laser illumination was provided by a custom-built laser combiner module (modification of LMM-3; Spectral Applied Research) containing 500-mW solid state lasers (488 nm [Coherent] and 561 nm [MPB Communications, Inc.]) that were shuttered with electronic shutters and attenuated and/or directed to a fiber-coupled output port with an Acousto optic tunable filter (Neos Technologies) and directed to the confocal scan-head via a single-mode optical fiber (Oz Optics). Time-lapse videos were acquired using a Coolsnap HQ2 cooled charge-coupled device camera (Photometrics) or a Clara cooled charge-coupled device camera (Andor Technology) operated in the 14-bit mode for 2 min at 2-s image intervals using a 300–400-ms exposure time. Microscope system automation was controlled with Metamorph software (Molecular Devices) or NIS Elements software (Nikon). Images of BFP-labeled constructs were taken using epifluorescent illumination using a filter set (ex/em 405/510) and exposure times of 800 ms. After acquisition, general image processing involved optimization of image brightness and contrast using the acquisition software package. Additional microscopy image manipulations and measurements are described in detail in the appropriate Materials and methods subsections.

Immunofluorescence. Fixation and processing of samples for immunofluorescence labeling was performed using a paraformaldehyde/glutaraldehyde coextraction/fixation buffer (PGF-PHEM; 4% paraformaldehyde, 0.15% glutaraldehyde, 0.2% Triton X-100 in 60 mM Pipes, 27.3 mM Hepes, 10 mM EGTA, and 8.2 mM $MgSO_4$, pH 7.0). PGF-PHEM was added to a coverslip with bound HUVECs at room temperature for 10 min, followed by rinsing (3 × 5 min) with 1× PBS (minus Ca^2 and Mg^2; HyClone), treated with 0.01 g/ml $NaBH_4$ in 1× PBS (2 × 15 min) to quench reactive aldehydes, rinsed once with 1× PBS, and finally blocked with 5% fat-free milk in 1× PBS (1 h at room temperature). Primary antibodies diluted in 1× PBS were added and incubated on a rocking platform overnight at 4°C (rabbit anti–pT288–Aurora A [1:1,000; Abcam] and rat anti–α-tubulin [1:500; AbD Serotec]). The next morning, the primary antibody was removed and the cells were rinsed 3 × 5 min in 1× PBS, followed by incubation in secondary antibodies in 5% fat-free milk (2 h at 37°C; Cy3 donkey anti-rabbit [1:1,000; Jackson ImmunoResearch Laboratories, Inc.] and Dyelight 649 goat anti-rat [1:1,000; Jackson ImmunoResearch Laboratories, Inc.]). Cells were mounted in mounting medium (Dako) and imaged on the TiE confocal spinning disk microscope.

Cell migration assay. Cell migration assays were performed on 22-mm round #1.5 coverslips prepared with fibronectin coating as described, but with the following modifications. Before plating the cells, the fibronectin-coated coverslips were dried using an aspirator. 500,000 transfected HUVECs were then cultured in 100 µl of EBM medium on the center of the dried coverslip to concentrate the cells and were allowed to adhere to the coverslip and form a confluent monolayer for 3–4 h. The monolayer was then rinsed two times in EBM medium to remove unattached cells and scraped with a razor blade to generate a wound edge. The cells were then allowed to recover in a 37°C incubator for 3 h before being assembled and mounted in a custom-built multiposition stage insert that allowed imaging of up to 12 coverslips per experiment. Phase-contrast images were acquired at 10-min intervals for 12 h on the microscope using a 10× 0.45 NA phase objective and a 0.52 NA LWD condenser using the Metamorph Multi-dimensional Acquisition (Molecular Devices) software module or using NIS Elements ND acquisition software module.

Quantification of cell branching and migration. For analysis of cell branching, fluorescent images of mApple-C1, a cell volume marker that aids in providing even illumination of the morphology of HUVECs, were used to allow for unbiased quantification. Branches were defined as protrusions that extended from the cell >10 µm in length and were counted only if they met this criterion. We defined the "branch origin" by locating the position on each side of the branch where the membrane displayed the greatest curvature and then connected those two points with a straight line. To measure branch length, the line tool in the Metamorph software or the line tool in the annotations and measurements application of NIS Elements software was used to measure the distance from the branch origin to the most distal point of the branch tip. Branch length measurements were recorded as the length of the "line" extending from the branch origin to the distal branch tip. Cell migration was quantified by hand-tracking the nucleolus in successive images from a time-lapse phase-contrast image series using the Track Points application in Metamorph or using the annotations and measurements application in NIS Elements software to determine instantaneous velocity and distance to origin. Statistical analysis was performed using the Analyze-It plug-in for Microsoft Excel (Analyze-It Software, Ltd.), and branching and migration data were compared using a Bonferroni-corrected, one-way analysis of variance test, with >95% confidence as the cutoff for statistical significance.

Colocalization analysis. For all colocalization analysis, single green channel (488 excitation) and red channel (561 excitation) images of HUVECs coexpressing Em–Aurora A and either mCherry-MCAK, mApple-EB3, or mApple-tubulin were acquired. A background region was selected from outside of the cell boundary for both channels and was subtracted from the original images. Within the subtracted red channel image only, the threshold function of Metamorph or NIS Elements software was used to exclude the fluorescent marker (respectively) and then the line tool in the annotations and measurements application of NIS Elements software was used to draw a 2-pt-thick line over the excluded object image. A 5-µm mask region of interest (ROI) was generated to define the leading and trailing edges as described (see MT dynamics analysis and Fig. 2). Once complete, the line objects from the red channel image were overlayed onto the Em–Aurora A image (green channel), and grayscale colocalization values as well as total Em–Aurora A values within the mask ROIs were recorded using the automated measurements application of NIS Elements software. Em–Aurora A colocalization values were calculated individually for each cell and then were grouped according to experimental treatment and subcellular region. Data are presented as the colocalized fraction of the total measured Em–Aurora A per subcellular region. Mean values for each group were compared statistically using the Analyze-It plug-in for

Microsoft Excel to perform a two-tailed student *t* test with 95% confidence as the cutoff for statistical significance.

MT dynamics analysis. MT dynamics were analyzed from EB3 videos using plusTipTracker software (Applegate et al., 2011), a Matlab-based, open-source software package that combines automated detection, tracking, analysis, and visualization tools for movies of fluorescently labeled MT plus end binding proteins (+TIPs). The +TIP comet detection algorithm relies on a watershed-based approach to estimate locally optimal thresholds. The track reconstruction algorithm uses the spatially and temporally globally optimized tracking framework described in Jaqaman et al. (2008), with cost functions modified to reflect MT track geometry. In brief, tracking occurs in two steps: frame-to-frame linking of comets into growth sub-tracks and the linking of collinear, sequential growth subtracks into compound tracks. The cost of joining two candidate growth sub-tracks into a compound track is calculated from three spatial parameters and one temporal parameter. After calculating the cost of linking all pairs of candidate growth tracks, the links are chosen by minimizing the global cost, which is achieved by solving the Linear Assignment Problem (Jaqaman et al., 2008).

Determination of image quality. Detection, tracking, and post-processing analysis were performed on the first 30 frames only for each movie, as photobleaching was a limiting feature in some conditions and movie length needed to be standardized for tracking comparison. The quality of the movies was assessed by examining comet detection performance; movies were discarded from further analysis if EB3 expression was too high and led to too many false positives or if focus drift or photobleaching led to a high standard deviation in mean comet number per frame over the course of the movie.

Tracking parameters. Tracking control parameters were optimized based on a parameter sweep using the plusTipParamSweepGUI tool of plusTipTracker (Applegate et al., 2011) and verified by visual inspection of track overlays on movies. The same parameter set was used for all movies in the dataset: maximum gap length, 12 frames; minimum track length, 3 frames; search radius range, 5–10 pixels; maximum forward angle, 25°; maximum backward angle, 8°; maximum shrinkage factor, 1.0; fluctuation radius, 2 pixels. For this study, only growth excursions were of interest, so MT shrinkage or pause events were not analyzed. However, sub-track linking was still performed to correct for the many occurrences when comets cross over one another or disappear momentarily from the field of view by focal drift, which breaks the trajectories prematurely.

Data grouping. PlusTipPickGroups function of plusTipTracker was used to create groups of data defined by experimental condition, resulting in a total of 20 experimental groups to be compared. From each group, cellular regions were defined (leading and trailing edge), resulting in a total of 40 groups to be compared (20 leading edge and 20 trailing edge). Groups ranged from 17–22 projects.

ROI selection. Binary masks of whole cell 5-µm cell peripheries and leading and trailing edges were generated in three steps using a modification of the plusTipTracker's sub-ROI selection tool. First, whole cell masks were manually selected based on the whole cell outlines as defined by phase-contrast images of wound-edge HUVECs. In the second step, cell periphery masks were automatically generated from whole cell masks by including all pixels within 5 µm of the cell edge. In the third step, leading and trailing edge masks were generated by manually drawing a 4-pt-thick line across the wound-edge cell of interest (see also Fig. 2). The subtraction of 5 µm of edge was accomplished by choosing the whole cell mask generated in the first step as an exclusion mask in the second. Regional areas were calculated by summing the area of the mask and converting to micrometers squared. The set of all MT growth excursions that spent ≥6 s (three frames) within the 5-µm ROI were extracted and stored within a subproject of the original cell.

MT growth sub-track subpopulation analysis

Tracks from within ROIs from all movies in the dataset were pooled using the plusTipPoolGroupData function to find the mean growth speed and mean growth lifetime. These values were used to split data for quadrant plot analysis (Applegate et al., 2011). Quadrant plot analysis was performed as separate batch processes for whole cell, leading edge, and trailing edge, thus defining for each of the groups the total number of tracks in each of four subpopulations: slow and short-lived, slow and long-lived, fast and short-lived, and fast and long-lived. The relative proportions of these four subpopulations were used to generate MT growth track overlays for visual comparison. Statistical comparison of MT growth speeds and growth lifetimes were performed using a permutation test for means using a threshold for statistical significance of $P < 0.001$.

Biochemistry

Western blotting. Cytoplasmic extracts from HUVECs were isolated in lysis buffer (50 mM Tris, pH 8.0, 150 mM NaCl, 0.5% sodium deoxycholate, and 1% Triton X-100). After lysis, cell nuclei were removed via centrifugation. Proteins from supernatants were quantified by the Bradford method. 10 µg of proteins were mixed with Laemmli sample buffer and separated by SDS-PAGE. After electrophoresis, proteins were electrotransferred to an immobilon-P membrane. For protein detection, membranes were blocked for 2 h at room temperature with 4% BSA in TBS-T buffer (20 mM Tris, pH 7.6, 137 mM $NaCl_2$, and 0.1% Tween-20) and incubated overnight at 4°C with mouse anti-MCAK (1:75; Abcam), rabbit anti–pT288–Aurora A (1:300, Abcam), mouse GFP (1:2,000; Abcam), mouse GAPDH (1:2,000; Abcam), mouse tubulin (1:1,000; DM1A; Cell Signaling Technology), or mouse anti–Aurora A (1:1,000; Abcam). After primary antibody incubation, blots were washed five times with TBS-T (3 min each) and incubated with the appropriate HRP-conjugated secondary antibodies (1:5,000; Jackson Immunoresearch Laboratories, Inc.) for 1 h at 37°C. Blots were washed five times (3 min each) with TBS-T and protein bands were visualized using an ECL detection system (SuperSignal West Pico Chemiluminescent Substrate; Thermo Fisher Scientific). For analysis of ECL, digital images of Western blot bands were quantified with ImageJ software (National Institutes of Health) after performing local background subtraction around bands of interest.

Immunoprecipitation. HUVECs were harvested in 150 µl NP-40 lysis buffer containing protease inhibitor (Thermo Fisher Scientific) and 100 mM NaFL to inhibit phosphatase activity. 100 µl of total protein extract was precleared with anti–mouse (TrueBlot Reagents; Rockland Inc.) or anti–rabbit IgG immunoprecipitation beads (TrueBlot Reagents), preclearing beads were pelleted, and supernatants were incubated with 1 µg of primary antibody (mouse anti-GFP, 1:2,000; Abcam; mouse anti-MCAK, 1:100; Abcam; or mouse anti-GAPDH (1:2,000; Abcam) and rotated 1 h at 4°C. Then, the solution was incubated with 100 µl of the appropriate immunoprecipitation beads (TrueBlot Reagents) with rotation at 4°C overnight. Beads were washed five times with lysis buffer, resuspended in 60 µl of Laemmli sample buffer, and boiled for 5 min. Samples were separated by running on a 4–12% precast tris-glycine polyacrylamide gel (Novex Tris-Gly Gels; Life Technologies) and then analyzed by Western blotting using the same antibodies as for the Western blots with the exception of GFP, which was blotted using a rabbit monoclonal antibody (1:5,000; Abcam). For loading controls, total lysate was run on a 4–12% gel. All primary antibody incubations were followed by incubation-appropriate secondary HRP antibodies (1:5,000; Jackson ImmunoResearch Laboratories, Inc.), and chemiluminescent visualization of protein bands was performed using ECL reagents (Thermo Fisher Scientific) according to the manufacturer's protocol.

For Western blotting and immunoprecipitation experiments, probing of the membrane with a second or third primary antibody was accomplished by first rinsing the membrane 3 × 5 min in TBS-T to inactivate the ECL reagent, followed by stripping of the primary antibody using incubation for 45 min at 70°C in stripping buffer (62.5 mM Tris, pH 6.8, 100 mM BME, and 2% SDS). After incubation in stripping buffer, the membrane was rinsed under running deionized water for 2 h and then washed 3 × 5 min in TBST to remove all traces of BME. The membrane was then blocked and incubated with primary and secondary antibodies.

Online supplemental material

Fig. S1 shows a summary of MT growth and cell behavior for all MT populations and experimental groups analyzed. Fig. S2 shows a summary of MT growth excursions for all leading and trailing edge MT populations and experimental groups analyzed. Video 1 shows live-cell imaging of MCAK tracking with growing EB3-labeled MT plus ends in HUVECs. Video 2 shows live-cell imaging of Aurora A tracking with MCAK-labeled MT plus ends. Video 3 shows live-cell imaging of Aurora A and tubulin in HUVECs expressing a CA-Rac1. Video 4 shows live-cell imaging of Aurora A and tubulin in HUVECs expressing a DN-Rac1. Online supplemental material is available at http://www.jcb.org/cgi/content/full/jcb.201401063/DC1.

We thank Linda Wordeman for providing MCAK constructs and Erich Nigg for providing Aurora A cDNA constructs, Bill Shin for imaging assistance and for maintenance of the microscope, Sergey Plotnikov for assistance with MatLab, Robert Fischer and Ana Pasapera for assistance with biochemical analysis, and all members of the Waterman laboratory for critical analysis and helpful discussion.

This work was supported by the National Heart, Lung and Blood Institute (NHLBI) Intramural Research Program (C.M. Waterman and K.A. Myers) and by Academic Career Award funding from the National Institutes of Health,

NHLBI (grant number 4K22HL113069-02; to K.A. Myers). A. Braun was supported by the College of Graduate Studies, University of the Sciences, and K. Dang and F. Buslig were supported by the Department of Biological Sciences, University of the Sciences.

The authors declare no competing financial interests.

Submitted: 16 January 2014
Accepted: 29 May 2014

References

Ahmad, F.J., T.P. Pienkowski, and P.W. Baas. 1993. Regional differences in microtubule dynamics in the axon. *J. Neurosci.* 13:856–866.

Akhmanova, A., C.C. Hoogenraad, K. Drabek, T. Stepanova, B. Dortland, T. Verkerk, W. Vermeulen, B.M. Burgering, C.I. De Zeeuw, F. Grosveld, and N. Galjart. 2001. Clasps are CLIP-115 and -170 associating proteins involved in the regional regulation of microtubule dynamics in motile fibroblasts. *Cell*. 104:923–935. http://dx.doi.org/10.1016/S0092-8674(01)00288-4

Al-Bassam, J., and F. Chang. 2011. Regulation of microtubule dynamics by TOG-domain proteins XMAP215/Dis1 and CLASP. *Trends Cell Biol.* 21:604–614. http://dx.doi.org/10.1016/j.tcb.2011.06.007

Andrews, P.D., Y. Ovechkina, N. Morrice, M. Wagenbach, K. Duncan, L. Wordeman, and J.R. Swedlow. 2004. Aurora B regulates MCAK at the mitotic centromere. *Dev. Cell*. 6:253–268. http://dx.doi.org/10.1016/S1534-5807(04)00025-5

Applegate, K.T., S. Besson, A. Matov, M.H. Bagonis, K. Jaqaman, and G. Danuser. 2011. plusTipTracker: Quantitative image analysis software for the measurement of microtubule dynamics. *J. Struct. Biol.* 176:168–184. http://dx.doi.org/10.1016/j.jsb.2011.07.009

Bayless, K.J., and G.A. Johnson. 2011. Role of the cytoskeleton in formation and maintenance of angiogenic sprouts. *J. Vasc. Res.* 48:369–385. http://dx.doi.org/10.1159/000324751

Brummelkamp, T.R., R. Bernards, and R. Agami. 2002. A system for stable expression of short interfering RNAs in mammalian cells. *Science*. 296:550–553. http://dx.doi.org/10.1126/science.1068999

Dehmelt, L., and S. Halpain. 2004. Actin and microtubules in neurite initiation: are MAPs the missing link? *J. Neurobiol.* 58:18–33. http://dx.doi.org/10.1002/neu.10284

Dehmelt, L., P. Nalbant, W. Steffen, and S. Halpain. 2006. A microtubule-based, dynein-dependent force induces local cell protrusions: Implications for neurite initiation. *Brain Cell Biol.* 35:39–56. http://dx.doi.org/10.1007/s11068-006-9001-0

Dent, E.W., and K. Kalil. 2001. Axon branching requires interactions between dynamic microtubules and actin filaments. *J. Neurosci.* 21:9757–9769.

Dent, E.W., J.L. Callaway, G. Szebenyi, P.W. Baas, and K. Kalil. 1999. Reorganization and movement of microtubules in axonal growth cones and developing interstitial branches. *J. Neurosci.* 19:8894–8908.

Desai, A., S. Verma, T.J. Mitchison, and C.E. Walczak. 1999. Kin I kinesins are microtubule-destabilizing enzymes. *Cell*. 96:69–78. http://dx.doi.org/10.1016/S0092-8674(00)80960-5

Fischer, R.S., M. Gardel, X. Ma, R.S. Adelstein, and C.M. Waterman. 2009. Local cortical tension by myosin II guides 3D endothelial cell branching. *Curr. Biol.* 19:260–265. http://dx.doi.org/10.1016/j.cub.2008.12.045

Fischer, R.S., K.A. Myers, M.L. Gardel, and C.M. Waterman. 2012. Stiffness-controlled three-dimensional extracellular matrices for high-resolution imaging of cell behavior. *Nat. Protoc.* 7:2056–2066. http://dx.doi.org/10.1038/nprot.2012.127

Ganem, N.J., K. Upton, and D.A. Compton. 2005. Efficient mitosis in human cells lacking poleward microtubule flux. *Curr. Biol.* 15:1827–1832. http://dx.doi.org/10.1016/j.cub.2005.08.065

Gerhardt, H., and C. Betsholtz. 2005. How do endothelial cells orientate? *EXS*. 94:3–15.

Gerhardt, H., M. Golding, M. Fruttiger, C. Ruhrberg, A. Lundkvist, A. Abramsson, M. Jeltsch, C. Mitchell, K. Alitalo, D. Shima, and C. Betsholtz. 2003. VEGF guides angiogenic sprouting utilizing endothelial tip cell filopodia. *J. Cell Biol.* 161:1163–1177. http://dx.doi.org/10.1083/jcb.200302047

Gerhardt, H., C. Ruhrberg, A. Abramsson, H. Fujisawa, D. Shima, and C. Betsholtz. 2004. Neuropilin-1 is required for endothelial tip cell guidance in the developing central nervous system. *Dev. Dyn.* 231:503–509. http://dx.doi.org/10.1002/dvdy.20148

Gundersen, G.G., Y. Wen, C.H. Eng, J. Schmoranzer, N. Cabrera-Poch, E.J. Morris, M. Chen, and E.R. Gomes. 2005. Regulation of microtubules by Rho GTPases in migrating cells. *Novartis Found. Symp.* 269:106–116, discussion :116–126: 223–230. http://dx.doi.org/10.1002/047001766X.ch10

Hunter, A.W., M. Caplow, D.L. Coy, W.O. Hancock, S. Diez, L. Wordeman, and J. Howard. 2003. The kinesin-related protein MCAK is a microtubule depolymerase that forms an ATP-hydrolyzing complex at microtubule ends. *Mol. Cell*. 11:445–457. http://dx.doi.org/10.1016/S1097-2765(03)00049-2

Jaqaman, K., D. Loerke, M. Mettlen, H. Kuwata, S. Grinstein, S.L. Schmid, and G. Danuser. 2008. Robust single-particle tracking in live-cell time-lapse sequences. *Nat. Methods*. 5:695–702. http://dx.doi.org/10.1038/nmeth.1237

Kita, K., T. Wittmann, I.S. Näthke, and C.M. Waterman-Storer. 2006. Adenomatous polyposis coli on microtubule plus ends in cell extensions can promote microtubule net growth with or without EB1. *Mol. Biol. Cell*. 17:2331–2345. http://dx.doi.org/10.1091/mbc.E05-06-0498

Kline-Smith, S.L., and C.E. Walczak. 2002. The microtubule-destabilizing kinesin XKCM1 regulates microtubule dynamic instability in cells. *Mol. Biol. Cell*. 13:2718–2731. http://dx.doi.org/10.1091/mbc.E01-12-0143

Knowlton, A.L., W. Lan, and P.T. Stukenberg. 2006. Aurora B is enriched at merotelic attachment sites, where it regulates MCAK. *Curr. Biol.* 16:1705–1710. http://dx.doi.org/10.1016/j.cub.2006.07.057

Kumar, P., K.S. Lyle, S. Gierke, A. Matov, G. Danuser, and T. Wittmann. 2009. GSK3β phosphorylation modulates CLASP-microtubule association and lamella microtubule attachment. *J. Cell Biol.* 184:895–908. http://dx.doi.org/10.1083/jcb.200901042

Lan, W., X. Zhang, S.L. Kline-Smith, S.E. Rosasco, G.A. Barrett-Wilt, J. Shabanowitz, D.F. Hunt, C.E. Walczak, and P.T. Stukenberg. 2004. Aurora B phosphorylates centromeric MCAK and regulates its localization and microtubule depolymerization activity. *Curr. Biol.* 14:273–286. http://dx.doi.org/10.1016/j.cub.2004.01.055

Lee, T., K.J. Langford, J.M. Askham, A. Brüning-Richardson, and E.E. Morrison. 2008. MCAK associates with EB1. *Oncogene*. 27:2494–2500. http://dx.doi.org/10.1038/sj.onc.1210867

Littlepage, L.E., H. Wu, T. Andresson, J.K. Deanehan, L.T. Amundadottir, and J.V. Ruderman. 2002. Identification of phosphorylated residues that affect the activity of the mitotic kinase Aurora-A. *Proc. Natl. Acad. Sci. USA*. 99:15440–15445. http://dx.doi.org/10.1073/pnas.202606599

Lorenzo, C., Q. Liao, M.A. Hardwicke, and B. Ducommun. 2009. Pharmacological inhibition of aurora-A but not aurora-B impairs interphase microtubule dynamics. *Cell Cycle*. 8:1733–1737. http://dx.doi.org/10.4161/cc.8.11.8617

Maney, T., A.W. Hunter, M. Wagenbach, and L. Wordeman. 1998. Mitotic centromere-associated kinesin is important for anaphase chromosome segregation. *J. Cell Biol.* 142:787–801. http://dx.doi.org/10.1083/jcb.142.3.787

Matov, A., K. Applegate, P. Kumar, C. Thoma, W. Krek, G. Danuser, and T. Wittmann. 2010. Analysis of microtubule dynamic instability using a plus-end growth marker. *Nat. Methods*. 7:761–768. http://dx.doi.org/10.1038/nmeth.1493

Mennella, V., G.C. Rogers, S.L. Rogers, D.W. Buster, R.D. Vale, and D.J. Sharp. 2005. Functionally distinct kinesin-13 family members cooperate to regulate microtubule dynamics during interphase. *Nat. Cell Biol.* 7:235–245. http://dx.doi.org/10.1038/ncb1222

Moore, A.T., K.E. Rankin, G. von Dassow, L. Peris, M. Wagenbach, Y. Ovechkina, A. Andrieux, D. Job, and L. Wordeman. 2005. MCAK associates with the tips of polymerizing microtubules. *J. Cell Biol.* 169:391–397. http://dx.doi.org/10.1083/jcb.200411089

Myers, K.A., I. Tint, C.V. Nadar, Y. He, M.M. Black, and P.W. Baas. 2006. Antagonistic forces generated by cytoplasmic dynein and myosin-II during growth cone turning and axonal retraction. *Traffic*. 7:1333–1351. http://dx.doi.org/10.1111/j.1600-0854.2006.00476.x

Myers, K.A., K.T. Applegate, G. Danuser, R.S. Fischer, and C.M. Waterman. 2011. Distinct ECM mechanosensing pathways regulate microtubule dynamics to control endothelial cell branching morphogenesis. *J. Cell Biol.* 192:321–334. http://dx.doi.org/10.1083/jcb.201006009

Nishimura, Y., K. Applegate, M.W. Davidson, G. Danuser, and C.M. Waterman. 2012. Automated screening of microtubule growth dynamics identifies MARK2 as a regulator of leading edge microtubules downstream of Rac1 in migrating cells. *PLoS ONE*. 7:e41413. http://dx.doi.org/10.1371/journal.pone.0041413

Ohi, R., T. Sapra, J. Howard, and T.J. Mitchison. 2004. Differentiation of cytoplasmic and meiotic spindle assembly MCAK functions by Aurora B-dependent phosphorylation. *Mol. Biol. Cell*. 15:2895–2906. http://dx.doi.org/10.1091/mbc.E04-02-0082

Pakala, S.B., V.S. Nair, S.D. Reddy, and R. Kumar. 2012. Signaling-dependent phosphorylation of mitotic centromere-associated kinesin regulates microtubule depolymerization and its centrosomal localization. *J. Biol. Chem.* 287:40560–40569. http://dx.doi.org/10.1074/jbc.M112.399576

Rannou, Y., M.B. Troadec, C. Petretti, F. Hans, S. Dutertre, S. Dimitrov, and C. Prigent. 2008. Localization of aurora A and aurora B kinases during interphase: role of the N-terminal domain. *Cell Cycle*. 7:3012–3020. http://dx.doi.org/10.4161/cc.7.19.6718

Rizk, R.S., K.P. Bohannon, L.A. Wetzel, J. Powers, S.L. Shaw, and C.E. Walczak. 2009. MCAK and paclitaxel have differential effects on spindle microtubule organization and dynamics. *Mol. Biol. Cell*. 20:1639–1651. http://dx.doi.org/10.1091/mbc.E08-09-0985

Rodriguez, O.C., A.W. Schaefer, C.A. Mandato, P. Forscher, W.M. Bement, and C.M. Waterman-Storer. 2003. Conserved microtubule-actin interactions in cell movement and morphogenesis. *Nat. Cell Biol.* 5:599–609. http://dx.doi.org/10.1038/ncb0703-599

Schulze, E., and M. Kirschner. 1988. New features of microtubule behaviour observed in vivo. *Nature*. 334:356–359. http://dx.doi.org/10.1038/334356a0

Tanenbaum, M.E., L. Macurek, B. van der Vaart, M. Galli, A. Akhmanova, and R.H. Medema. 2011. A complex of Kif18b and MCAK promotes microtubule depolymerization and is negatively regulated by Aurora kinases. *Curr. Biol.* 21:1356–1365. http://dx.doi.org/10.1016/j.cub.2011.07.017

Teerawanichpan, P., T. Hoffman, P. Ashe, R. Datla, and G. Selvaraj. 2007. Investigations of combinations of mutations in the jellyfish green fluorescent protein (GFP) that afford brighter fluorescence, and use of a version (VisGreen) in plant, bacterial, and animal cells. *Biochim. Biophys. Acta*. 1770:1360–1368. http://dx.doi.org/10.1016/j.bbagen.2007.06.005

van der Vaart, B., A. Akhmanova, and A. Straube. 2009. Regulation of microtubule dynamic instability. *Biochem. Soc. Trans.* 37:1007–1013. http://dx.doi.org/10.1042/BST0371007

van der Vaart, B., M.A. Franker, M. Kuijpers, S. Hua, B.P. Bouchet, K. Jiang, I. Grigoriev, C.C. Hoogenraad, and A. Akhmanova. 2012. Microtubule plus-end tracking proteins SLAIN1/2 and ch-TOG promote axonal development. *J. Neurosci.* 32:14722–14728. http://dx.doi.org/10.1523/JNEUROSCI.1240-12.2012

Van Veen, M.P., and J. Van Pelt. 1994. Neuritic growth rate described by modeling microtubule dynamics. *Bull. Math. Biol.* 56:249–273. http://dx.doi.org/10.1007/BF02460642

Wadsworth, P. 1999. Regional regulation of microtubule dynamics in polarized, motile cells. *Cell Motil. Cytoskeleton*. 42:48–59. http://dx.doi.org/10.1002/(SICI)1097-0169(1999)42:1<48::AID-CM5>3.0.CO;2-8

Walczak, C.E., T.J. Mitchison, and A. Desai. 1996. XKCM1: a *Xenopus* kinesin-related protein that regulates microtubule dynamics during mitotic spindle assembly. *Cell*. 84:37–47. http://dx.doi.org/10.1016/S0092-8674(00)80991-5

Waterman-Storer, C.M., R.A. Worthylake, B.P. Liu, K. Burridge, and E.D. Salmon. 1999. Microtubule growth activates Rac1 to promote lamellipodial protrusion in fibroblasts. *Nat. Cell Biol.* 1:45–50. http://dx.doi.org/10.1038/9018

Wittmann, T., and C.M. Waterman-Storer. 2005. Spatial regulation of CLASP affinity for microtubules by Rac1 and GSK3β in migrating epithelial cells. *J. Cell Biol.* 169:929–939. http://dx.doi.org/10.1083/jcb.200412114

Wittmann, T., G.M. Bokoch, and C.M. Waterman-Storer. 2003. Regulation of leading edge microtubule and actin dynamics downstream of Rac1. *J. Cell Biol.* 161:845–851. http://dx.doi.org/10.1083/jcb.200303082

Wittmann, T., G.M. Bokoch, and C.M. Waterman-Storer. 2004. Regulation of microtubule destabilizing activity of Op18/stathmin downstream of Rac1. *J. Biol. Chem.* 279:6196–6203. http://dx.doi.org/10.1074/jbc.M307261200

Wordeman, L., M. Wagenbach, and G. von Dassow. 2007. MCAK facilitates chromosome movement by promoting kinetochore microtubule turnover. *J. Cell Biol.* 179:869–879. http://dx.doi.org/10.1083/jcb.200707120

Zhang, X., W. Lan, S.C. Ems-McClung, P.T. Stukenberg, and C.E. Walczak. 2007. Aurora B phosphorylates multiple sites on mitotic centromere-associated kinesin to spatially and temporally regulate its function. *Mol. Biol. Cell*. 18:3264–3276. http://dx.doi.org/10.1091/mbc.E07-01-0086

Zhang, X., S.C. Ems-McClung, and C.E. Walczak. 2008. Aurora A phosphorylates MCAK to control ran-dependent spindle bipolarity. *Mol. Biol. Cell*. 19:2752–2765. http://dx.doi.org/10.1091/mbc.E08-02-0198

Zhao, Z.S., J.P. Lim, Y.W. Ng, L. Lim, and E. Manser. 2005. The GIT-associated kinase PAK targets to the centrosome and regulates Aurora-A. *Mol. Cell*. 20:237–249. http://dx.doi.org/10.1016/j.molcel.2005.08.035